

Quantum Dot-Sensitized Solar Cells

P. Sudhagar, Emilio J. Juárez-Pérez, Yong Soo Kang
and Iván Mora-Seró

Abstract Quantum dot sensitized solar cells, but in general semiconductor sensitized photovoltaic devices, have erupted in recent years as a new class of systems, differentiated for several reasons of the most common dye-sensitized solar cells. In this chapter, we review the enormous potentialities that have impelled the research in this field. We highlight the differences between quantum dot and dye-sensitized solar cells that we divide in five aspects: (i) Preparation of the sensitizer; (ii) Nanostructured electrode; (iii) Hole Transporting Material; (iv) Counter electrode, and (v) Recombination and surface states. Some of the optimization works performed in each one of these lines is revised, observing that further improvement can be expected. In fact, the recent breakthrough in photovoltaics with organometallic halide perovskites, originated by the intensive study on quantum dot-sensitized solar cells, is also revised, stressing the potentiality of these systems for the development of low cost photovoltaic devices.

1 Introduction

Since the apparition of the Homo Sapiens in Africa, 200,000 years ago, the evolution of the society has been closely linked to an increment of the energy consumption. From the early days of the hunters and harvesters society to the current industrial societies the energy consumption per person and day and the world population have both experienced an exponential growth [1]. The demand for

P. Sudhagar · Y. S. Kang
World Class University Program Department of Energy Engineering and Center for Next Generation Dye-Sensitized Solar Cells, Hanyang University, Seoul 133-791, South Korea

E. J. Juárez-Pérez · I. Mora-Seró (✉)
Photovoltaic and Optoelectronic Devices Group, Departament de Física, Universitat Jaume I, 12071 Castelló, Spain
e-mail: sero@uji.es

power during the last period of industrialization is compensated with the use of nonrenewable sources, fossil fuels such as coal and oil. Their use not only represents an irreplaceable depletion of stocks, avoiding its use on other beneficial issues especially in the case of oil, but it has caused serious side effects as the greenhouse effect. Gases from combustion have a potentially catastrophic impact in the global warming and the climate change as it has been recognized since the end of the twentieth century by the United Nations [2]. In this sense, energy has become one of the most striking problems of the humankind. It is easy to recognize that the energy problem is not only important in itself but for its implications in many of the great challenges of humanity in the twenty-first century (wars, environment, food, water...). This situation strongly demands a change in the weighting of the different energy sources in the energy cocktail that powers the world. The weight of nonrenewable energy sources necessarily has to decrease, even if this decrease is unintentional due to the stock reduction. It is debatable whether the size of the nonrenewable energy source reserves is large or small, but the irrefutable fact is that these reserves are finite. On the other hand, to maintain the economic development the energy consumption cannot be significantly decreased, and the reduction of energy from nonrenewable sources has to be compensated with power coming from renewable sources.

Undoubtedly photovoltaic energy is the renewable power source with higher potentiality, as the Earth receives from the Sun in just 1 hour the same amount of energy that it is expended by all the humankind in 1 year [3]. But the devices that we currently have to harvest energy from this huge pool, they are expensive compared to other energy sources. In this sense, a reduction of cost in photovoltaic devices is mandatory to take full advantage of the tremendous potentialities of these systems. There are two ways to attain this scope: (i) reducing the fabrication cost of the device; (ii) increase the efficiency of the photovoltaic devices. To attain both solutions nanoscience can help us.

The new technologies capable of constructing material structures with dimensions from 0.1 to 50 nm have opened numerous possibilities to investigate new devices in a domain heretofore inaccessible to the investigators and technologists. A considerable activity exists in nanoscience and technology in university and industrial laboratories around the world. The requirements of improved efficiency and versatility, and of reduced cost of the photovoltaic devices, have led to search for extending the field of traditional study in inorganic semiconductors, incorporating new materials, and structures capable of satisfying these requirements. In the field of the photovoltaic solar power, the challenge of the future for the new concepts on nanoscale is to reduce the present cost of the devices by a factor 10–100. Candidates to lead this revolution are the new nanocomposite solar cells, formed by coatings deposited from liquid solutions. These procedures avoid the need of treatment in vacuum, and improve substantially the time and cost of production. Also the highly energetic stages of the process of production are avoided, improving the time of recovery of the spent energy. With the advanced optimization on nanoscale, and the application of solution low cost, it is possible to achieve the efficient use of minuscule quantities of matter.

Nanoscale considerations have been also important implications in the development of low cost photovoltaic devices, from the point of view of the fundamental principles. Conventional Si solar cells rely on high quality materials since the carriers generated in the device after photon absorption remain in the same material until they are extracted at the selective contacts [4]. This involves the use of sophisticated technologies with high production cost in order to avoid carrier recombination before their extraction. Conversely, nanoscale absorbers can quickly separate the photogenerated carriers into two different media which allows for a less-demanding materials quality and therefore cost reduction, as transport of electrons and holes is occurring in different materials and recombination is reduced. These are the fundamentals of the new paradigm introduced to the photovoltaic conversion by the sensitized solar cells that have received a major attention since the seminal paper of O'Regan and Grätzel at the beginning of the 1990s [5]. Most of the work carried out in sensitized solar cells has been made using organic and/or metalorganic molecular dyes acting as light absorbing materials. The use of inorganic semiconductors as nanoscale light harvesters has been minority. But the undoubted photovoltaic properties of these materials have pushed the research in this field with a continuous growing interest in the last few years. This interest has resulted in a constant growth of the reported efficiencies. This fact with the easy preparation and its low cost make of the inorganic semiconductor sensitized solar cells one of the fields of photovoltaics that is experienced higher growth. This chapter is devoted to the study of these systems focusing mainly in two aspects the low cost preparation and the role of nanoscale design and the advanced structures for solar cell preparation

This chapter is structured in nine sections. The first one is this brief introduction. In the second, we analyze the fundamentals of sensitized solar cells, explaining the specificities of dye, semiconductor, and quantum dot solar cells, and reviewing the state of the art. In Sect. 3, the experimental techniques used for semiconductor light absorbing material deposition are revised, stressing the fact of their low cost and easy industrial implementation. In the fourth part, new promising substrate structures in the case of inorganic semiconductor absorber are revised, in order to highlight the role of nanoscale and the possibilities of design. In Sect. 5, the hole transporting material is revised for both liquid electrolytes of all solid devices. In Sect. 6, the counter electrode material is determined by the hole transporting material and proper choice has to be done as we analyze in this section. In the seventh, the effect of carrier recombination before being collected at the output terminals, the role of surface states in the light absorbing materials has overviewed. In the penultimate part, a new class of light absorbing materials "halide perovskites" has arisen and made revolution in this field. Despite there are several proves indicating that this kind of devices are not fully behaving as a sensitized device, it has been the intense work in sensitized solar cells that have allowed to achieve this breakthrough. Therefore, we consider that it is important to include these systems in this chapter. This new hot topic in photovoltaics is also taking benefit of the knowledge and characterization techniques developed in the last decades for sensitized devices. Finally, very briefly conclusions are highlighted.

2 Sensitized Solar Cells

As commented in the introduction the fundamentals of sensitized solar cells is to decouple light absorption and charge transports making that these processes occur in different media. When light is absorbed by molecular dyes the devices are called Dye-Sensitized Solar Cells (DSSCs), and are the most extensively studied class of sensitized devices [6]. But here we are going to focus our attention in the case where inorganic semiconductor are used as light absorbing materials instead of dyes giving place to the Semiconductor-Sensitized Solar Cells (SSSCs) [7]. When the size of the semiconductor material is small enough to observe effects due to quantum confinement (particle radius lower than the Bohr radius) the devices is called Quantum Dot-Sensitized Solar Cells (QDSSCs) [8–10]. The line separating SSSCs from QDSCs is fuzzy and many times the denomination QDSSCs is preferred even in cases where quantum confinement is not observed.

The working principle of QDSSCs is fundamentally similar to DSSCs and they are represented in Fig. 1. A wide bandgap semiconductor material is sensitized with an semiconductor with a bandgap in the visible or near IR region. The most extensively used wide bandgap semiconductor has been TiO_2 , but several examples of the utilization of other ones as ZnO [11] or SnO_2 [12–14] have been reported. Light irradiation photo excites electron-hole pairs from the QD Valence Band (VB) to the QD Conduction Band (CB). Photoexcited carries are injected into two different transporting media. Electrons are injected into the CB of the wide bandgap semiconductor, while hole are injected into a hole transporting material (HTM). Then both carriers diffuse to their respective contacts. In order to optimize cell performance, recombination of diffusing carriers should be avoided. As the light absorbing layer is extremely thin effective surface area is significantly enhanced with the use of a nanostructured electrode, increasing consequently the light harvesting [5]. This description is perfectly valid also for DSSCs. In this sense, in a first analysis it could be thought that semiconductor QDs are only one more of the thousand of dyes that have been checked in DSSCs. But we want to highlight here that it is not the case. The different nature of QDs in comparison with molecular dyes makes that the complete design of the solar cell device have to be rethought.

Main differences between DSSCs and QDSSCs could be divided into five aspects:

- (i) Preparation of the sensitizer.
- (ii) Nanostructured electrode.
- (iii) Hole Transporting Material (HTM).
- (iv) Counter electrode.
- (v) Recombination and surface states.

In the next five sections, we will develop each of these points reviewing the current state of the art of QDSSCs.

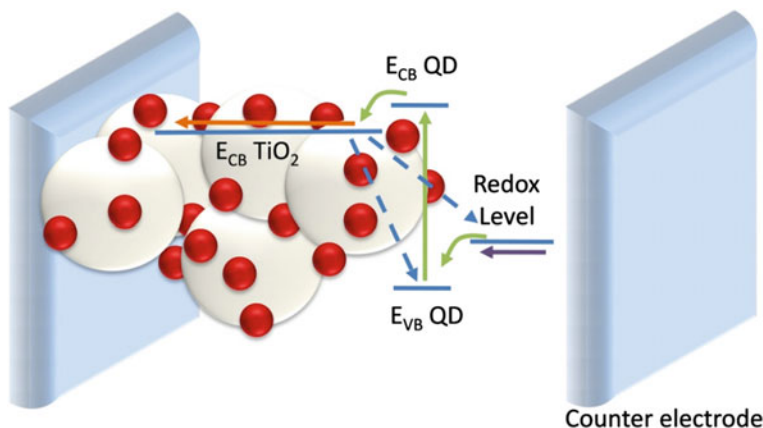


Fig. 1 Cartoon representing the fundamental principles of sensitized solar cells. Light photoexcites electron-hole pairs at the QD (vertical *green arrow*). Photoexcited electron is injected into the CB of the wide bandgap semiconductor, while hole is regenerated from the redox level of the liquid electrolyte (or the VB of a solid hole transporting material). Electron in wide bandgap semiconductor is transported to the electron contact (*orange arrow*). Redox system is regenerated at the counter electrode and electrons diffuse to the working electrode (*purple arrow*). During the transport process electron can recombine with holes in the QDs or in the HTM (*blue dashed arrows*)

3 Sensitization with Inorganic Semiconductor Quantum Dots

Considering the sensitized synthesis, an inorganic semiconductor can be prepared by several ways and the growth mechanism determines dramatically the performance of the photovoltaic device [15, 16]. In this chapter, we want to highlight the potentiality of QDSSCs for the development of low cost photovoltaic devices. In particular, we will review some of the techniques, most commonly, employed for the sensitization with inorganic semiconductors. Interestingly, these techniques do not require any special experimental conditions like vacuum or high temperatures; this fact is especially attractive for industrial development as it is an effective way for cost reduction.

Two major strategies have been practically used to sensitize QDs onto the electrodes (a) in situ preparation of QDs on the electrode surface and (b) attachment of presynthesized Colloidal Quantum Dots (CQDs) on the electrode surface. The former method includes chemical bath deposition, [17] successive ionic layer adsorption/reaction, [18] electrochemical deposition, [19] and photochemical deposition [20]. The latter exploits, but is not limited to, linker molecules, [8, 21–23] direct absorption, [16, 22, 24] spray pyrolysis deposition, [25, 26], and electrophoretic deposition [27–30]. There are also some examples of the combination of these two approximations [31, 32].

The use of CQDs allows the production of material with a high degree of crystallinity a high control of QD properties (as size, shape, bandgap...) but in the first reports relatively low QD loading was obtained [16, 22]. In QDSSCs, it is widely reported historically that directly grown QDs on the electrode surface show relatively high performance than that of indirectly attached CQDs, due to a higher sensitizer loading and consequently higher harvesting efficiency [16, 33]. Using direct assembled approach, the QDs were attached to mesoporous framework robustly and charge transfer resistance was possibly reduced [34, 35]. But it was demonstrated that potentially QDSSCs based on CQDs exhibit a higher potentiality for the development of efficient devices [16]. Semiconductor grown directly on the surface of the mesoporous electrode present poor crystallinity and broader quantum dot size dispersion than CQDs. In addition, deleterious effects in the grain boundaries could arise [7]. Recently, the group of Zhong has developed a method based in a ligand exchange of the capping molecules in CQDs [36–38]. With this method higher QD loading is attained and consequently higher efficiency in fact the record efficiency for QDSSCs has been reported by this group with $\text{CdSe}_x\text{Te}_{1-x}$ CQDs [38].

Taking into account these considerations here we review different sensitization methods for both CQDs and semiconductors grown directly on the electrode surface. The following coating methods were identified as low cost methods compared to physical and vacuum techniques:

3.1 Sensitization with Colloidal Quantum Dots

For the sensitization with CQDs two consecutive steps are required. In first step, presynthesized CQDs are grown with an accurate control of the crystalline quality, size, and shape (and consequently bandgap) distribution or capping [39]. Second, CQDs should be attached to the nanostructured electrode. However, there is no single procedure to attach CQDs to the photoanode and it is possible to differentiate between assisted and direct sensitization. In the assisted sensitization process, bifunctional linker molecules are used to anchor CQDs to the nanostructured photoanode [8, 23]. These linker molecules generally have a functional carboxylic group which first attach to one side of the TiO_2 and the other side of the linker (generally a thiol group) was connected to the CQD [8, 23]. In addition to carboxyl linkers, other functional groups can also be applied as bifunction linkers for fixing CQD to the nanoporous electrode (as amine group in cysteine), and is realized that this linker molecules play an important role in PEC performance [21]. On the other hand, CQDs can be directly attached to the electrode without the use of any specific linker. For example, if toluene solvent for CdSe CQDs is substituted by dichloromethane, CQDs can be directly absorbed on TiO_2 surface simply by dipping the substrate in the dichloromethane solution with CQDs [22, 24]. The use of linker molecules is benefit during the CQDs synthesis which capped with, generally, long organic molecules (oleic acid), thus offer controlling QD size and

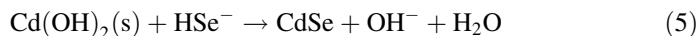
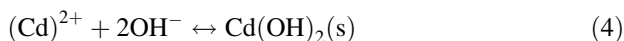
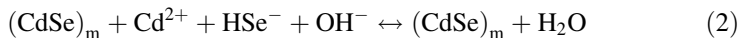
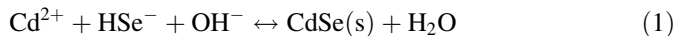
avoid agglomeration [39]. It has been shown that the ligand exchange helps anchoring QDs to mesoporous electrode, for example, TOPO molecules coating CdSe QDs were substituted by pyridine in order to enhance the QD loading of sensitized electrode [40]. This strategy has been employed with significant success by the group of Zhong, where oleic acid is substituted by mercaptopropionic acid (MPA) [41]. Then aqueous solution with MPA-capped QDs is pipetted directly on the electrode surface, where it stayed for 2 h before rinsing sequentially with water and ethanol and then drying with nitrogen. This procedure has produced QDSSCs with efficiencies higher than 5 % [36, 37] or even 6 %, [38] as it has been already commented.

The methods presented so far have the drawbacks that need long duration for sensitization in most of the cases, as the dipping process to attach the linker molecule and/or the QDs requires several hours for an optimum loading [8]. Sensitization time can be significantly reduced by employing the electrophoretic technique. Basically, in this technique an electrical field is applied between two electrodes dipped in a QD solution. Ionized QDs are attracted to the electrodes and attached in one or both electrodes [42]. CQD deposition rate on the mesoporous electrode depends on the applied voltage, high CQD loading can be obtained in few hours [28, 29] or even in few minutes [27]. Even, electrophoresis has been used to attach rod shape sensitizers (nanorods) to TiO₂ electrodes, [29] to prepare electrodes with QDs of different sizes [30] or to assemble CdSe QDs and fullerene for an innovative solar cell [43]. Nevertheless the efficiencies reported for QDSSCs using electrophoresis are shown below the performance reported for other attaching modes with CQDs.

3.2 Chemical Bath Deposition

The second main approximation for the sensitization with inorganic semiconductor is direct growth of light absorbing material on the surface of the wide bandgap semiconductor electrode. The remaining section will be dedicated to this last approximation with three low cost techniques that will be overviewed: (a) Chemical bath deposition (b) successive ionic layer adsorption and reaction (SILAR), and (c) electrodeposition. Chemical bath deposition (CBD) is a convenient method to assemble the QDs on a variety of substrates (conducting and nonconducting) at elevated temperatures compared with most other semiconductor QDs deposition methods [44]. The simplicity of CBD process together with the inherent low temperature operations results in superior control over the QDs particle size [17]. Several articles explain the variety of QDs assembly by CBD method, i.e., CdS, [18, 45, 46] CdSe, [34, 47, 48] Sb₂S₃ [49–52], CdTe, [53–56] PbS [27, 57–60], etc. The two main mechanisms for the CBD process are (1) ion-by-ion deposition onto a coating surface without bulk precipitation in the deposition solution and (2) bulk precipitation (or colloid formation) with diffusion of the bulk semiconductor clusters to the coating surface [44]. The complex agents were usually utilized to

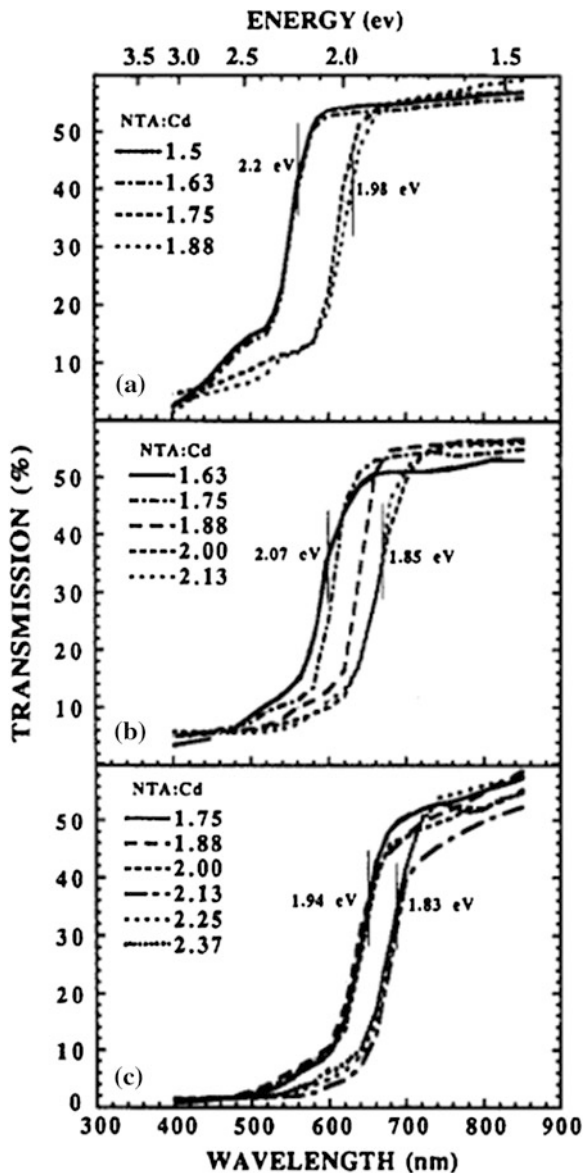
maintain the pH of the chemical bath, which directly control the reaction rate and hence overcome the bulk precipitation in the chemical bath [61]. For example, the reaction mechanism of in situ coating of CdSe QDs onto mesoporous TiO₂ is explained as follows: [62]



Reactions (1)–(2) describe the formation of CdSe without the formation of Cd(OH)₂ seed layer. Subsequently, Cd²⁺ and Se²⁻ species are forming larger clusters by coalescence or aggregation with other clusters (3). Coalescence refers to a combination of two clusters to form one single crystal, while aggregation means the formation of two or more separate but contacting crystals. The latter was suggested to be the terminating step in crystal growth for CBD CdSe films. As for CdSe, the reverse direction of reaction (5) will lead to redissolution of the solid phase and will control the size of the Cd(OH)₂ crystallites (i.e., colloidal particles) in the solution. Thus, lower temperatures result in a higher concentration of small Cd(OH)₂ nuclei and results in the formation of CdSe crystal with smaller size. The effect of Se²⁻ ions at a Cd(OH)₂ surface will be replaced by a selenide due to much lower solubility of CdSe compared with Cd(OH)₂. The Cd(OH)^{*} nucleus will eventually be converted to CdSe (reaction 1). Thus, the reaction will continue by formation of hydroxide and its subsequent conversion into CdSe (4 and 5). Therefore, the nucleation process on coating surface takes vital role in determining QDs formation mechanism, which is often controlled by precursor concentration and chemical bath temperature and is explained elsewhere by Gorer et al. [62] (Fig. 2). Different QD size, as can be deduced from the different bandgap, can be obtained by varying temperature and concentration in the CBD process, see Fig. 2.

The typical chemical bath deposition of CdSe QDs is as follows [63, 64]: a chemical bath solution was prepared by mixing 80 mM CdSO₄ and 80 mM sodium selenosulfite (Na₂SeSO₃) solution with 120 mM nitrioloacetic acid. The mesoporous TiO₂ electrodes were immersed in the chemical bath at 10 °C for 12 hours. Finally, the films were soaked in deionized water and dried with nitrogen. Recently, antimony sulfide (Sb₂S₃) QDs sensitizers prepared by CBD method showed efficient PCE performance 4–5 % in both liquid-type and solid-state hybrid solar cells [65–68]. Deposition of Sb₂S₃ coating by CBD is cheaper than the other available techniques. Typical coating of Sb₂S₃ QDs is explained elsewhere [67, 68]. Briefly, the mixture of 1 M solution of SbCl₃ in acetone and 1 M Na₂S₂O₃ cold aqueous solution addition with cold water is adjusted to have a final

Fig. 2 Optical transmission spectra of CdSe films deposited at various temperatures (a) 10 °C (b) 40 °C, and (c) 80 °C with various NTA:Cd ratios (NTA: nitrilo triacetic acid applied as complex agent) (Reprinted permission with Gorer et al. [62])



concentration of Sb^{3+} and S_2O_3 of ~ 0.025 and ~ 0.25 M, respectively. The CBD solution is quickly poured in the CBD recipient, where the electrodes were placed vertically, and the recipient was left in a refrigerator at ~ 7 °C for 2 h. Then, the samples are rinsed with deionised water and dried by flowing nitrogen. Efficiencies as high as 6.3 % have been reported in all-solid QDSSCs with Sb_2S_3 [67].

From the earlier reports, it is found that the deposition of QDs by CBD method densely covers the mesoporous metal oxide surface and enhances the recombination resistance [10, 63, 69, 70]. Despite the effective coverage on TiO_2 surface, CBD method generally result in nanocrystalline films pattern rather than particles coating. Therefore, it is mostly suitable for wide-pore-nanostructured electrodes (nanotube, nanowire, nanotube, and inverse opal) [71]. The nanocrystalline film coatings may block the narrow pore-channel of conventional nanoparticulate electrodes having limited pore size (5–7 nm). Also, this method takes several hours for coating (12–48 h) and high roughness surface requires seed layers, for example CdS is widely applied as seed layer for CdSe deposition [64].

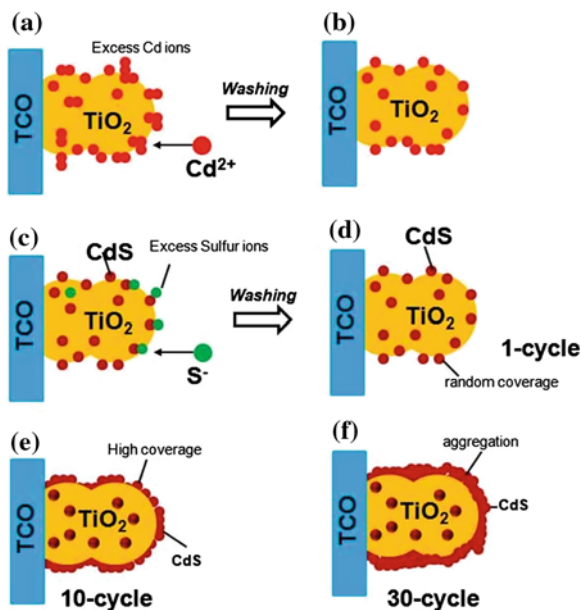
3.3 *Successive Ionic Layer Adsorption and Reaction (SILAR)*

The successive ionic layer adsorption and reaction (SILAR) method is an emerging method for depositing variety of semiconductor quantum dots both as binary (CdS, CdSe, PbS, CdTe, CuS, Sb_2S_3 , Sb_2Se_3 , Bi_2S_3 , etc.) and ternary compounds ($\text{CdS}_x\text{Se}_{1-x}$, CuInS, CuIn_2S_3 etc.) [72, 73]. The SILAR method is inexpensive, simple and convenient for large area deposition. There is no restriction of coating surface and can be widely applied to all kind of materials such as insulators, semiconductors, and metals. One of the advantages of SILAR process is the likelihood of achieving coatings at low temperature which avoids oxidation and corrosion of the substrate. The following parameters are indispensable in controlling the particle size and bandgap of QDs; concentration of the precursors, nature of complexing agent, pH of the precursor solutions and adsorption, reaction, and rinsing time durations etc. [74]. The reviews by Mane et al. [44] and Pawar et al. [75] provide the detailed picture of semiconducting chalcogenide films coating by SILAR. The growth mechanism involves four most important steps: (a) specific adsorption of cationic precursor (b) rinsing of the nonspecifically adhered chemicals, and (c) the chemical reaction between the most strongly specific adsorbed cations and less strongly adsorbed anions by the subsequent substrate immersion in the anion solution; and (d) rinsing of the species that did not react. These four steps constitutes a SILAR cycle, it can be repeated many times, increasing each time the amount of deposited material. Various stages of QDs growth (for example CdS QDs) is explained in Fig. 3. The average QD size can be controlled by the number of deposition cycles. This method has been used specifically to prepare metal sulfides, but recently SILAR process is expanded to prepare a variety of metal selenides and tellurides [76].

In SILAR method, the particle size of QDs is controlled by number of coating cycles. The number of coating cycles depends on the concentration of chemical bath. As explained in CBD method, increasing the bath concentration above the critical concentration (R_c) limits the number of SILAR cycles where the QDs are

Fig. 3 Schematic illustration of SILAR process

(a) Adsorption of cationic ions (Cd^{2+}) (b) rinsing (I) removes excess, nonspecifically adsorbed Cd^{2+} (c) reaction of anionic (S^{2-}) with preadsorbed Cd^{2+} ions to form CdS and (d) rinsing (II) to remove excess and unreacted species and form the solid solution CdS on surface of the substrate. The coverage of CdS at higher cycles (e) 10 and (f) 30



redissolved into chemical bath and QDs films might peel-off from the coating surface. During first SILAR cycle, the seed layer of QDs was formed on the coating surface and directing further growth for successive coating cycles. The influence of coating cycles on growth of QDs can be studied by optical absorption spectra. Figure 4a–c explains the influence of coating cycles on optical absorption of CdS, CdSe [77], and Sb_2S_3 [78], respectively. From Fig. 4a, it is clearly understood that the absorption of CdS and CdSe is found to increase by gradually improving the coating cycles. Interestingly, nucleation and growth of CdSe on TiO_2 can be greatly accelerated with a CdS underlayer, where CdS is rather a promoter for the preferential growth of CdSe (Fig. 4b) as it has been also observed for CBD.

Typically, semiconductor QDs by SILAR process has been demonstrated under aqueous medium, but the high surface tension causes poor wetting ability on a solid surface, which leads to poor penetration of the solution in a porous matrix. Therefore, low surface tension solvent is recommended like alcohol solutions for efficient QDs coating. Since it has high wettability and superior penetration ability on the mesoscopic TiO_2 film, well-covered QDs on the surface of mesopores is achieved easily. The high coverage of QDs results by alcohol solvent showed high absorbance than that of aqueous solvent (Fig. 4c).

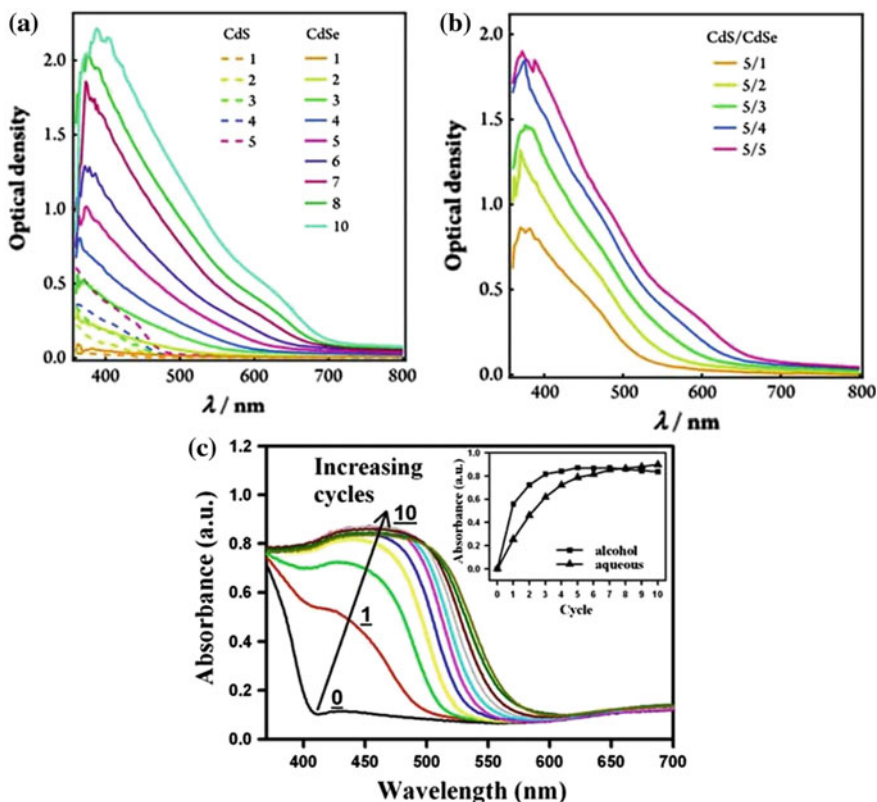


Fig. 4 UV-visible optical density (OD) spectra of as-prepared (a) nCdS and nCdSe, and (b) 5CdS/nCdSe-coated 2.4 mm TiO₂ electrodes, where n is the number of SILAR deposition cycles. The OD spectra represent the net light absorption by the sensitizers as the substrate absorption (mesoporous TiO₂) was subtracted from the absorption spectra of corresponding nCdS, nCdSe and 5CdS/nCdSe-sensitized TiO₂ electrodes [Hossian et al. reprinted with permission from RSC] [77] (c) UV-vis absorption spectra of TiO₂ with different coating cycles of CdS QDs in alcohol solutions. The inset shows the absorbance of excitonic peaks after various cycles of the CBD process for alcohol and aqueous systems [Chang et al. [45] reprinted permission from AIP publishers]

3.4 Electrodeposition

Electrodeposition (ED) is an emerging technique for synthesizing semiconductor thin films and nanostructures, especially chalcogenides and oxides [79–85]. One of the great advantages of ED method is that they are more suitable for solar cells application [86, 87] since it allows the possibility of easily altering both the bandgap and lattice constant by composition modulation through the control of growth parameters such as applied potential, pH, and temperature of the bath. Thus, it is at least in principle possible to easily grow large areas of tandem cells

designed for the most efficient conversion of the solar spectrum. A large number of semiconductors CdS, [19, 88] PbS, [89–91], and CdSe, [85, 92, 93] etc., have been electrodeposited with varying coating parameters such as electrolyte concentration, pH, and applied potential, etc. The ED method is restricted to electrically conductive materials. In the electrochemical deposition, the substrate (mesoporous TiO₂-coated TCO) is submerged in a liquid solution (electrolyte). When an electrical potential is applied between a conducting area of the substrate and a counter electrode (usually platinum) in the liquid, a chemical redox process takes place resulting in the formation of a semiconductor QDs layer on the substrate. The schematic of hybrid electrochemical/chemical deposition of CdS QDs are presented in Fig. 5 [94].

Recently, Wang group, [13] and X-Y Yu et al., [19] demonstrated the electrodeposition of CdSe QDs on SnO₂ and ZnO nanostructures, respectively. The completely covered CdSe QDs by electrodeposition on mesoporous SnO₂ photoanodes showed 17.4 mA cm⁻² with 3.68 % PCE, which is relatively a high performance compared to the previous reports on SnO₂ photoanodes-based QDSSCs. The growth methodology of electrodeposited CdSe QDs at different cycles is explained in Fig. 6. The size of QDs was influenced by number of coating cycles. However, more number of coating cycles may block the pores.

In this section, we have summarized the most important sensitization methods for QDSSCs. We observe the relative simplicity of the methods, that they do not require vacuum or high temperature conditions. Therefore, chemical approach of QDs sensitization method is inherently low cost and remarkable efficiency higher than 6 % has been reported. This fact advocates that QDSSCs have tremendous potential for the future development of low cost photovoltaic devices.

4 Photoanodes in QDSCs

The photoanode of a QDSSC functions as selective contact for electrons [4]. In addition, it also works as an electron “vehicle” to transport the injected electrons from the excited QDs sensitizers to the outer circuit. In general, the photoanode materials need to satisfy several properties: first, the energy gap of the semiconductor could match with that of the QDs-sensitizer to ensure an effective injection of the photo-induced electrons from the QDs to the semiconductor, ensuring in addition electron selectivity blocking holes. Second, the semiconductor electrode must have a high surface area to accommodate more QDs, so as to harvest as much photon as possible. The photoanode material is the indispensable component of QDSSCs which plays crucial role in sensitizer loading, electron injection, transportation, and collection, and therefore exhibits significant influence on the photocurrent, photovoltage, and the power conversion efficiency. Recently, remarkable efforts have been paid to the design of the chemical composition, structure, and morphology of the semiconductor photoanode.

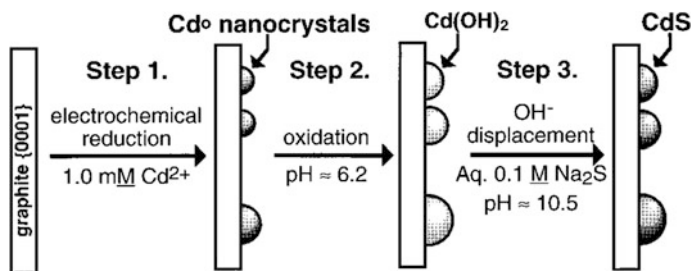


Fig. 5 Schematic diagram illustrating the three step electrochemical/chemical (E/C) synthesis of epitaxial CdS nanocrystals [Anderson et al. [94] Reprint permission from ACS]

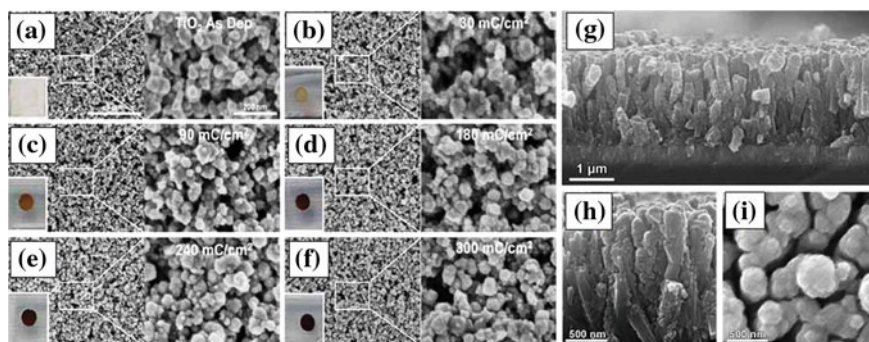
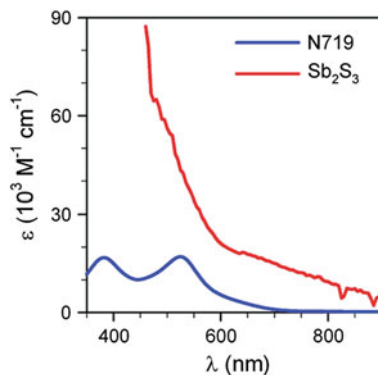


Fig. 6 SEM images of low and high magnification of CdSe-free mesoporous film of TiO₂ (a) and for different CdSe electrodeposition times from 30 to 300 mC cm² (b)–(f). [Sauvage et al. [183], reprint permission from IOP publishers]. (g)–(i) CdSe QDs electrodeposited TiO₂ rutile nanowires [Kamat et al. [184], reprint permission from Wiley VCH]

In sensitizer-type solar cells, the photoanode should have high surface area to accommodate more amount of sensitizer loading to enhance light harvesting. However, the recombination process is proportional to the electrode surface area. The open-circuit potential (V_{oc}) in sensitized solar cells is significantly affected by the recombination process. A balance between recombination and light harvesting is therefore needed to maximize sensitized solar cell performance. With these considerations on mind inorganic semiconductors are extremely attractive due to their high extinction coefficient, in many cases, see Fig. 7.

In Fig. 7, a comparison of the extinction coefficients of one of the most employed dyes in DSSCs, N719, with the inorganic semiconductor Sb₂S₃. This implied that the effective surface area of QDSSCs covered with QDs may not need as much increase as in DSSCs for achieving high light harvesting. In this sense, QDSCs can take advantage of the development of new electrode structures to control the recombination process with lower effective area and consequently lower recombination. In addition, despite the high extension coefficient of

Fig. 7 Extinction coefficient of molecular dye N719, one of the most popular dyes in DSSCs, and Sb_2S_3 inorganic semiconductor [Boix et al. [185] reprint permission from ACS]



semiconductor QDs sensitizers, it is relatively larger in size than dye molecules; therefore it is difficult to penetrate deeper parts of TiO_2 electrode and thus limiting the sensitizer loadings. Therefore, large-pore network is prerequisite to afford effective QDs loading. On the other hand, such photoanodes could demonstrate high charge transport from sensitizer to a charge collector, ultimately, overwhelming the charge recombination at photoanode/electrolyte interface. Therefore, to achieve (a) high sensitizer loading (b) fast electron transport channel, and (c) good electrolyte pore-filling, establishing multifunctional photoanode framework is the promising approach in QDs-sensitized solar cells. The following nanostructures has been identified as futuristic architectures in QDSSCs (a) highly interconnected, spatially assembled 1-D network (b) branched nanowires with highly conducting backbone which directly attached to charge collector, and (c) three-dimensionally ordered pore arrays with high scattering capability. Some of the electrode preparation methods also present a high interest for industrial application, as electrospinning.

In this context, nanofibrous membrane (NF), inverse opal (IO) and hierarchal nanowire (HN) electrodes receive great deal of attention as three-dimensional (3-D) photoanodes for next generation DSSCs or QDSSCs. In this section, we will discuss the fabrication and advantageous of 3-D nanostructured photoanodes in QDSCs.

4.1 Directly Assembled Continuous Fibrous Electrodes

Utilization of the wide pore-structured nanofibers is receiving great attention for superficial electrolyte penetration through their vertical pores yield effective interfacial contacts with TiO_2 -sensitizer interfaces [95, 96]. In particular, fibrous electrodes prepared by an electrospinning technique showed remarkable performance in DSSCs since it support large-scale anode fabrication at low cost. Archana et al. [97] reported that a 1-D fibrous film results in a high diffusion coefficient

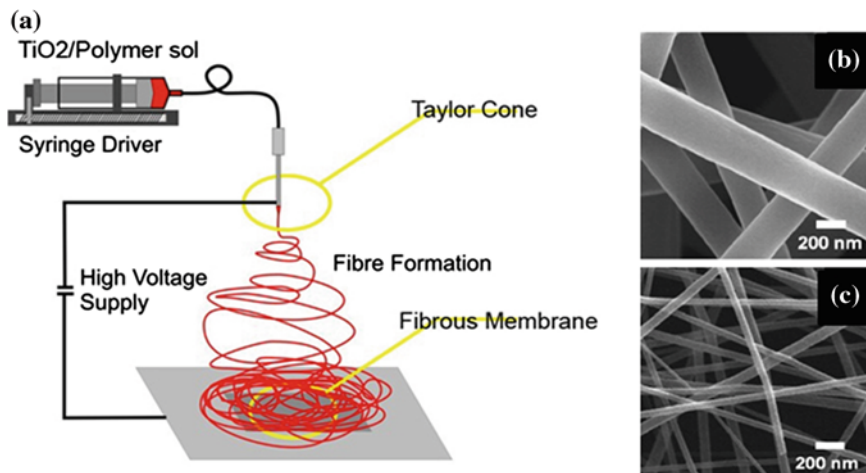


Fig. 8 a Schematic illustration of electrospinning set up. The TiO₂ fibrous channels were directly deposited onto collector (FTO substrates); SEM images of (b) as prepared TiO₂ fibers and (c) calcinated fibers (An et al. [186] Reprinted permission from Elsevier)

($D_n \approx 4.6 \times 10^{-4} \text{ cm}^2 \text{ s}^{-1}$), which is nearly 3 times higher than that of the particulate electrodes ($D_n \approx 1.5 \times 10^{-4} \text{ cm}^2 \text{ s}^{-1}$) under identical photoexcitation density. Furthermore, they observed less charge transport resistance and transit time in the fibrous electrode over the nanoparticle electrode. The high electron diffusive transport characteristics of fibrous electrodes are fostering as effective photoanodes for achieving feasible charge collection at QDSCs compared to conventional nanoparticle electrodes. In addition, fibers have less grain boundary density, which can overcome the trapping–detrapping loss unlike conventional nanoparticle electrodes and beneficial advantages in attenuating the scattering loss [98]. On the other hand, the inclusion of nanofibers in conventional nanoparticle electrodes (composite) substantially improves the light harvesting through promoting the light-scattering pattern (analogous to antenna lobes) [99]. The first QDs (CdS: CdSe)-sensitized solar cells using direct assembled 3-D fibrous electrodes has been demonstrated by Sudhagar et al. [47] Followed that significant work has been developed on fibrous QDSSCs. The schematic structure of electrospinning (ES) set up is shown in Fig. 8.

The detailed working principles of ES technique have been explained elsewhere [100–102]. Briefly a continuous TiO₂ fibrous membrane is directly assembled on a FTO substrate using the electrospinning technique (Fig. 8). The typical solution is used for spinning: 0.53 g of polyvinyl acetate (PVAc) dissolved in 4.45 g of dimethyl formamide (DMF). After completely dissolving the PVAc in DMF, 1 g of titanium(IV) propoxide and 0.5 g of acetic acid were mixed well for 30 minutes. The resultant solution for spinning is loaded into a syringe driver and connected to a high-voltage power supply. An electrical potential of 15 kV was applied over a collection distance of 12 cm. The electrospun fibrous membranes were collected

continuously on the grounded FTO substrate for 20 minutes. Subsequently, the films were sintered at 450 °C for 30 minutes in air. The diameter of the fibrous membranes can be easily modified by adjusting the Taylor cone size through (a) sol concentration (b) flow rate, and (c) applied potential.

Most fibrous electrodes have been fabricated using a two-step method. After fiber synthesis, substrates are coated with the synthesized fibers, but in this case poor particle interconnectivity is detected [96, 103]. Continuous electrospun fibers can solve this problem but peel off limitations has to be overcome. Various approaches have been demonstrated for this purpose. Song et al. utilized a hot press method to enhance the adhesion of the nanofiber to the substrate [95]. Similarly, chemical treatment was also employed to relax the nanofiber to yield an improved adhesion of the nanofiber to the substrate [104]. Onozuka et al. [105] applied a dimethyl formamide (DMF) treatment to TiO₂ fibrous electrodes, where DMF induced the swelling of the polymeric substances in the composite film and reinforced the adhesion between the substrate and fibrous membranes. This DMF treatment has improved the charge collection efficiency of DSCs by about 20 % compared to untreated electrodes. Analogous DMF-treated electrospun spheroidal electrodes were tested in QDSSCs, where the efficiencies increased from 0.85 to 1.2 % through improving the electrical contact between the fibers and the Transparent Conducting Oxide (TCO) substrate [106]. Despite the good electrical contact achieved by chemical treatment, it could affect the fibrous morphology thus lower the pore volume of the electrode, which severely affect the QDs loading and electrolyte penetration. In view of maintaining electrode pore volume as well as good electrical contact between TCO and fibrous network concurrently, it would be a better choice to choose chemical vapor treatment instead of direct chemical treatment.

Recently, we studied the above said hypothesis of surface treatment (chemical treatment and chemical vapor treatment) in fibrous electrodes and provide the detailed insights in controlling recombination rate at QDSCs [63]. Figure 9a–c compares the SEM images of different surface-treated TiO₂ fibrous electrodes. It clearly indicates that the untreated fibers (Fig. 9a), show a smooth surface with 70–100 nm diameters and several micrometers length. After surface pretreatment with DMF (Fig. 9b), the fibrous channels were intertwined and became a rather compact structure. This may be due to the fact that DMF treatment swells the polymer content of the fibers, thus resulting in a coagulated fiber structure. This coagulated fiber structure reduces the interpore distance between each fiber channel, reducing consequently the effective surface area of the electrode for electrolyte penetration. However, it could improve the electrical contact between the FTO substrate and the fibrous TiO₂ layer. In the case of tetrahydrofuran (THF) vapor treatment (Fig. 9c), the fibrous surface seems etched, which could consequently improve fibers inter-junction points. Also, the interpore distance between fibrous channels is partially retained after the THF pretreatment. As a consequence, THF treatment produces electrodes to half way between UT and DMF electrodes.

From Fig. 9d THF-QDSSCs result high open-circuit voltage $V_{oc} = 0.57$ V with slight improved short circuit photocurrent $J_{sc} = 9.74$ mA cm⁻² compares to untreated fibrous electrode based QDSSCs, while the DMF cell presents a lower

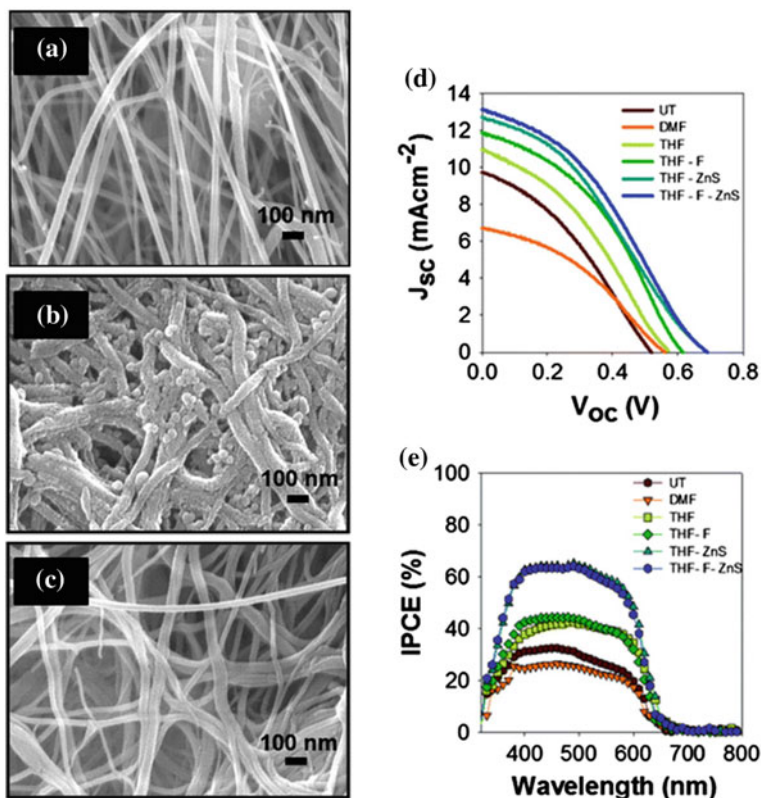


Fig. 9 SEM images of (a) untreated (b) DMF treated and (c) THF vapor-treated TiO₂ fibers; **d** current–voltage (J – V) measurements and (f) IPCE spectra of QDSSCs using different surface treated TiO₂ fibers electrodes. The electrode thickness is 2.4 μm . (Sudhagar et al. [63] reprint permission from RSC publishers)

photocurrent. The observed higher performance in THF vapor-treated cells may attribute to the improved physical adhesion of fibers with the TCO substrate. The recombination parameters of this system have been studied and found that chemical vapor treatment offer high charge recombination resistance to the electrodes. Interestingly, these TiO₂ fibrous membranes afford high feasibility in altering their Fermi level under post-doping process. Under the post-doping of fluorine ion (in Fig. 9d, THF+F) results upward Fermi level shift in TiO₂ conduction band. This Fermi level upward shift promotes the V_{oc} as well as fill factor (FF) of the device. We found that the combined pretreatment (THF) and post-treatment (F ion doping and ZnS QDs decoration on CdS/CdSe QDs) the 3-D TiO₂ fibrous photoanode yielded a device performance of 3.2 % with a remarkable $V_{oc} = 0.69$ V compared with most of the reports existing in the literature.

Yet another attempt on improving the electrical contact between fibrous electrode with TCO substrates has been demonstrated by Samadpour et al. [107].

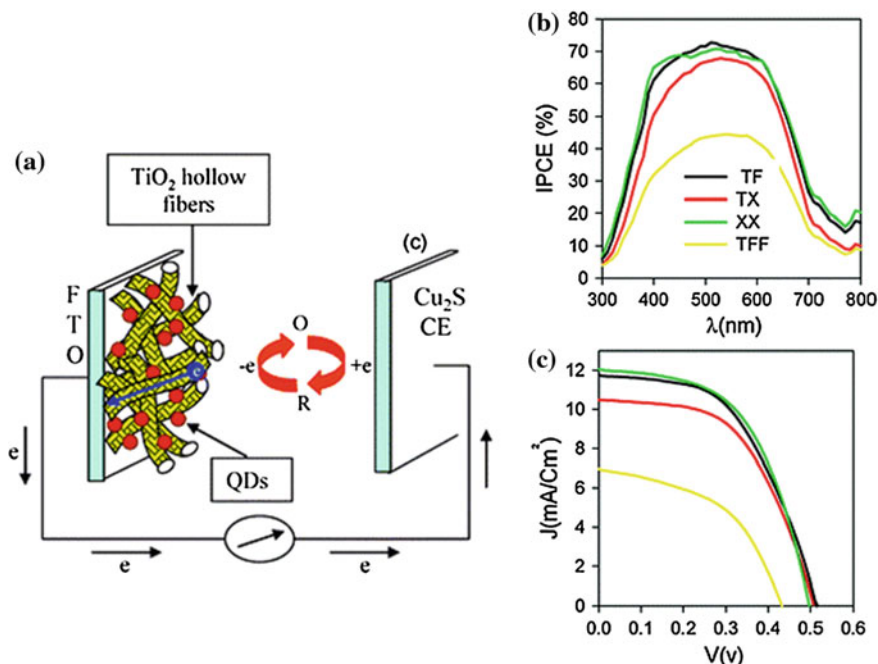


Fig. 10 a Schematic view of the hollow nanofibrous anode based QDSCs, IPCE; corresponding (b) IPCE and (c) J–V curves of the SILAR sensitized cells. (Samadpour et al. [107] reprint permission from RSC publishers)

They explored that the inclusion of nanoparticle glue layer in between the hollow nanofiber promotes the electrical contact between fiber channels with TCO as well as promote the surface area of the electrode. Figure 10 shows the schematic of hollow nanofiber photoanode-based QDSC (Fig. 10a) along with JV and IPCE performance (Fig. 10b, c). In this work, authors compared nine different photoanodes for instance conventional particulate TiO₂ (NP), pure hollow nanofiber (NF), and mixed composite of NP and NF. From Fig. 10b, c, the efficiency of the pure hollow fiber (F) structure is just 0.66 % ($V_{oc} = 0.43$ V, $J_{sc} = 3.1$ mA cm⁻², FF = 0.54), the efficiency of cells with XX structures (TiO₂ paste which contained TiO₂ nanoparticles and fibers) increased to 3.24 % (Fig. 10c), which constitutes a 6-fold enhancement. In this structure, the 20 nm nanoparticles act as a glue crosslinking the fibers and also improving the adhesion with the FTO substrate. Mixing both fibers and nanoparticles (X structures) has the additional beneficial effect of light scattering and facile electron transport provided by the one-dimensional hollow fiber structure. The TiO₂ paste which contained TiO₂ nanoparticles and fibers (XX) showed high performance than that of pure hollow fiber-based QDSSCs (data not shown in the figure).

Nevertheless the direct assembled fibers showed competitive performance with nanoparticulate structures, under similar thickness, further enhancing the electrode thickness (above 10 micron) is really a challenging task. Since, at high thickness

the fibrous membranes are found to peel off from the TCO substrate. Recently, we demonstrated the hierarchical hollow nanofibrous electrode with nanotube branches which balancing the trade-off between the fibrous thickness and mechanical stability [108]. Assembling NT arrays on a highly interconnected 3D fibrous backbone would reinforce the stability of the electrode. Figure 11 shows the fabrication stages of hierarchical 3-D hollow TiO₂ nanofibers (H-TiO₂-NFs) and the detailed experimental procedure explained in elsewhere [108].

Figure 12a shows the QD-sensitized 3-D TiO₂ nanotubes branched on TiO₂ hollow nanofibers (H-TiO₂ NFs). The high resolution TEM images reveal that the spatially decorated TiO₂ NT arrays on TiO₂ NFs have good contact with the TiO₂ backbone. Furthermore, TEM images (Fig. 12a, b) suggest that the TiO₂ tubular branches have sufficiently large pore channels for electrolyte filling as well as good structural stability. This 3-D photoelectrode was tested and compared with conventional vertically grown TiO₂ nanotube on TCO (TiO₂-NT). The optical reflectance spectra (Fig. 12c) shows high reflectance compared to TiO₂-NTs in the wavelength range of 380–800 nm. This might be attributed to the multiple scattering of incident light at the hierarchical TiO₂ NT branches, thus drastically enhancing the reflectance of the electrode. The photovoltaic performance of TiO₂-NT and 3-D H-TiO₂ NFs electrodes were compared in Fig. 12d. The TiO₂-NTs directly grown on a FTO electrode resulted in a photoconversion efficiency of $\eta = 0.9\%$ with photovoltage, $V_{oc} = 0.62$ V, photocurrent, $J_{sc} = 2.5$ mA cm⁻², and fill factor, FF = 58.3%. As anticipated, the hierarchical TiO₂ nanotube branches grown on a hollow NF backbone show unprecedentedly promoted to $\eta = 2.8\%$ with $V_{oc} = 0.61$ V, $J_{sc} = 8.8$ mA cm⁻² and F.F. = 50.3%. It is clearly evident that the TiO₂ NTs spatially assembled on the hierarchical 3D-nanofibrous backbone promote the QDSSC performance by a factor of three compared to the TiO₂ NTs directly grown on a TCO substrate. We can relate the enhancement of photocurrent generation with the H-TiO₂ NF photoanodes to several contributions: (a) higher effective surface area and consequently higher QD loading and light harvesting; (b) highly efficient charge collection throughout the photoanode with fewer boundary layers and (c) the multiple scattering effects of the comb-like hierarchical NT arrays, in particular, red photon harvesting.

4.2 3-D Tree-Like Branched Hierarchical Nanowire

Designing vertically grown 1-D nanostructures such as nanowire [109–112] and nanotube [113–117] which directly attached to the charge collectors (TCO) provides high charge collection efficiency in DSSCs. However, the larger voids presence in between the nanowire/tube channels lowers the internal surface area of the electrode [118]. Promoting internal surface area through introducing hierarchal branches on 1-D nanostructured stems are beneficial approach for achieving 3-D photoanodes and offers simultaneously improved surface area and favorable electron transportation. The resultant 3-D complex nanoarchitectures show many

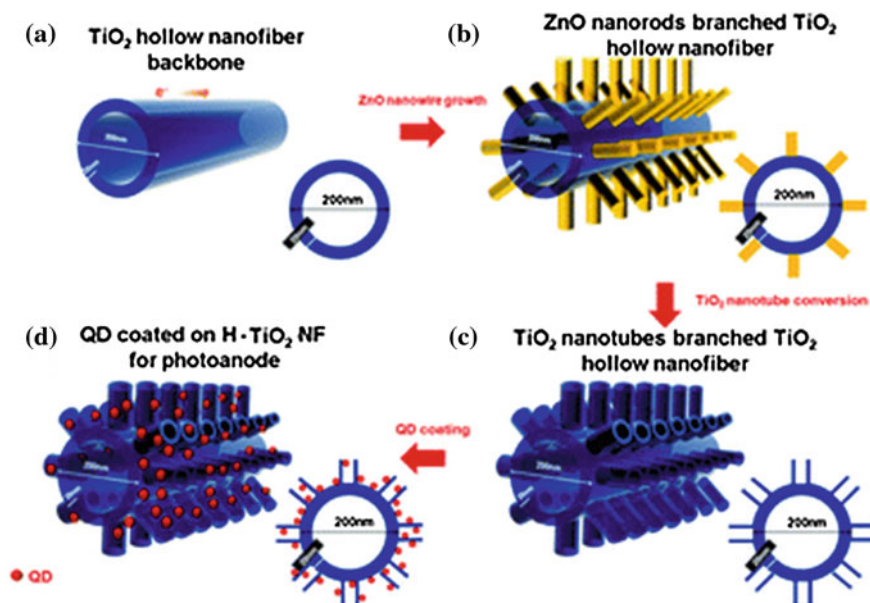


Fig. 11 Schematic illustration of H-TiO₂ NF photoanode fabrication stages of (a) TiO₂ hollow nanofibers (TiO₂-NFs), (b) ZnO NR templates grown on TiO₂-HNFs, (c) TiO₂ nanotube branches grown on TiO₂-NFs through ZnO NR templates, and (d) QD-sensitized H-TiO₂ NF photoanode. (Han et al. [108] reprint permission from RSC publishers)

advantages in sensitizer-type solar cells including: (i) the enhancement in the light-harvesting probability through large surface area for sensitizer loading and photon localization arising from the random multiple scattering of the light within the pine tree network (ii) the direct charge extraction pathways throughout the device thickness (fast electron transport from sensitizer to collecting terminal), and (iii) the huge 3-D porous network that allows better electrolyte filling, with possible beneficial implications for preparation of solid devices.

Among the many 3-D hierarchical anode architectures, “tree-like” morphology is a versatile candidate, since the tree-like configuration can be fabricated in large scale and each electronic interfaces being assembled at separate stages without any complication. The schematic structure of proximally coated sensitizers on tree-like framework is illustrated in Fig. 13. Under irradiation the excited electrons at sensitizer can inject to wide bandgap branches (WB-PA), and subsequently the electrons were being rapidly reached to collector substrate through conducting backbone nanowire (stem) [119].

Macroscopically, assembling tree-like crystalline framework results 3-D “nanoforest” structure, which offer ample room for more quantity of sensitizer loading compare to branch-free nanowire electrodes. This approach is simply mimicking branched plant structures, ultimately, to capture more sunlight.

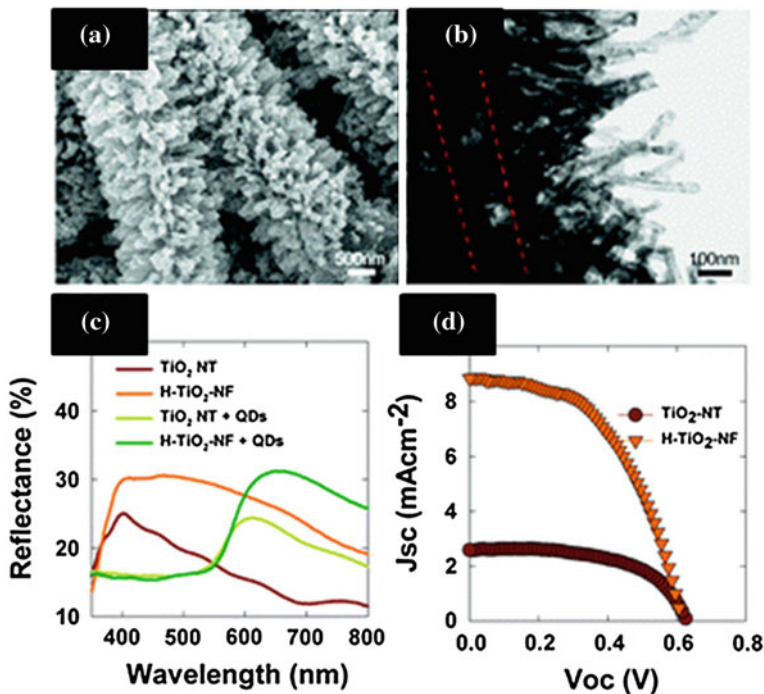


Fig. 12 a FE-SEM and b HR-TEM images of H-TiO₂ NF; c diffused reflectance spectra and d J-V plots of QDS-sensitized TiO₂ nanostructures. (Han et al. [108] reprint permission from RSC publishers)

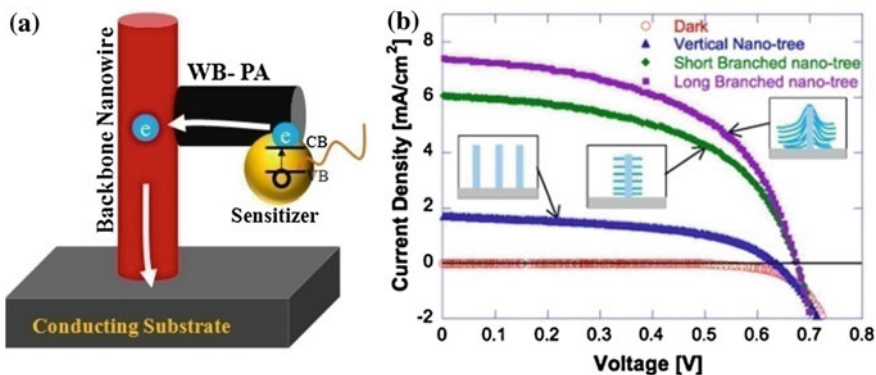


Fig. 13 a Schematic structure of electronic interfaces in 3-D tree-like photoanodes; b the J-V performance of branched nano-tree photoanodes compares with branch-free TiO₂ photoanodes (Herman et al. [187] reprint permission from IOP publishers)

Figure 13b clearly explains the advantage of tree-like photoanodes compared to conventional nanowire electrodes. From Fig. 13b the photocurrent of the DSSC has monotonically increased by extending the length of branches in the electrode. The similar photocurrent enhancement in hierarchical 3-D tree-like photoanodes has been widely found in the DSSCs literature [120–122]. The efficiency enhancement of 3-D tree-like electrodes is mainly due to enhanced surface area enabling higher sensitizer loading and light harvesting and also is due to reduced charge recombination by direct conduction along the stem of the nano-tree [123]. The hierarchical branches in tree-like electrodes has been grown either by seed layer-assisted method, [124–126] or self-catalyst-based mechanism [127]. The stem of the electrode (back bone) may be nanowire or nanotube. However, the overall photoconversion efficiency of the 3D tree-like photoanode strongly depends on their growth mechanism. Wu et al. compared the performance of hierarchical TiO₂ nanowire array photoanodes (hydrothermally grown without seed layer) with P25 nanoparticle under similar dye uptaking condition [127]. The J_{sc} and V_{oc} of P25-based DSSC is 12.0 mA·cm⁻² and 794 mV, respectively, which is much lower than those of 3hr grown hierarchically TiO₂ nanowire arrays (13.9 mA·cm⁻² and 826 mV). By increasing the branch length through increasing hydrothermal duration time to 9 h, the efficiency of the device promotes to 7.34 %. Further extending nanowire branch growth duration to ~12 h the conversion efficiency found to be decreasing to 6.35 %, which may be ascribed to the formation of more recombination pathways at nanowire/electrolyte interfaces which lower the conversion efficiency of the device. Interestingly, diffusion coefficient of iodine redox shuttle is ~2 orders higher in hierarchical nanoforest electrodes ($D(I_3^-) = 3.3 \times 10^{-8}$ cm²/s) than NP electrode ($D(I_3^-) = 5.4 \times 10^{-10}$ cm²/s) [128]. It is understood that the enhanced mass transport of the redox shuttle anticipated to result high V_{oc} in the device and is realized in many tree-like anode-based DSSCs.

Recently, we demonstrated the QDSSCs with high open-circuit voltage as high as 0.77 V in ZnO nanowires array electrodes [70]. The performance of the cell can even be increased to a promising 3 %, using a novel photoanode architecture of “pine tree” ZnO nanorods (NRs) on Si NWs hierarchical branched structure. The different stages of fabricating hierarchical ZnO nanorods on Si backbone nanowires are schematically shown in Fig. 14.

The typical experimental procedure of pine tree-like Si/ZnO electrodes is as follows: in first stage, the backbone Si nanowires were fabricated via the vapor-liquid-solid (VLS) process on the Au nanoparticle decorated FTO glass by using a chemical vapor deposition (CVD) system. By introducing a 10 % silane (SiH₄) in Hydrogen (H₂) mixture in a tube furnace, Si nanowires were synthesized under the reactor temperature and pressure were kept at 480–520 °C and 40 torr for 3 min. This Si NW thickness is assumed as total thickness of the photoanode. The n-type doping of Si NWs was achieved by using PH₃ gaseous precursor as in situ doping sources. A more detailed description of the Si NWs growth conditions and their electrical characteristics can be found elsewhere [70]. At second stage, ZnO hierarchical rods were grown on Si NWs. The 25 nm thick ZnO film, as a seed layer, was deposited on FTO glass by using magnetron sputtering. The sample was

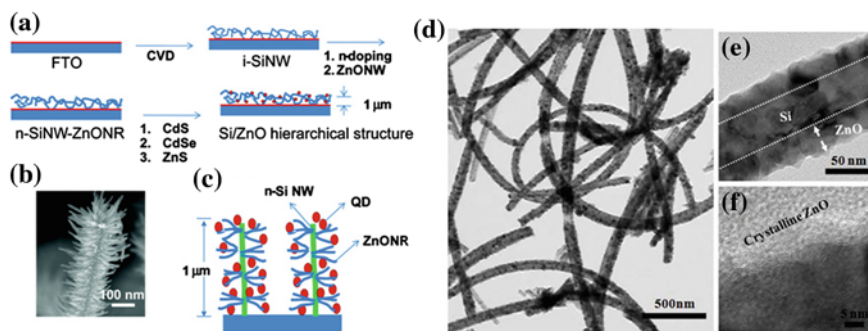


Fig. 14 **a** Fabrication scheme of Si/ZnO hierarchical structure **b** SEM image of n-Si-NW/ZnO-NR, and **c** schematic Si/ZnO hierarchical structure for photoanode **d** HRTEM images of ZnO seed-coated Si Nanowire, and **e** and **f** their corresponding high magnification TEM images. (Sudhagar et al. [70] ©Reprint permission from ACS Publishers)

transferred to a beaker containing 25 mM zinc nitrate and 25 mM methenamine in water for the growth of ZnO NWs and was kept in the oven at 85 °C. After 12 h, the electrodes were removed from the beaker and rinsed with water then dried by N₂. The ZnO NWs present an average length and diameter of 2.2–2.5 μm and 100–150 nm, respectively. Figure 14d, e shows the TEM images of bare and ZnO seed particle coated Si nanowire, respectively.

Figure 15a clearly depicted that the branched ZnO NRs directly grown on the Si-NWs forming a pine tree structure. HR-TEM image (Fig. 15b) at the top of ZnO NRs reveals that the ZnO NRs are single crystalline and were grown along the [001] direction. The porosity of the electrode has been maintained even after QDs coating (Fig. 15c), which is beneficial for effective electrolyte penetration through entire device. The optical reflectance property of ZnO-NR and 3-D n-Si-NW/ZnO-NR HBS has been studied by diffuse reflectance (Fig. 15e). Both sensitized electrodes present a decrease in the reflectance for the wavelength shorter than 620 nm due to light absorption of CdS/CdSe sensitizer. Analyzing the reflectance values at longer wavelength, before the absorption threshold, the improved scattering properties of the pine tree HBS, in comparison with ZnO NWs, are manifested in the higher reflection values at these wavelengths. The IPCE presents (Fig. 15f) a similar threshold to reflectance. It is important to highlight that no significant IPCE is observed at wavelengths longer than 700 nm, indicating a negligible contribution of the Si-NWs to QDSC performance. This fact also suggests that the light absorbed by Si-NWs is negligible and consequently the differences observed in reflectance values at longer wavelength in (Fig. 15e) are in fact due to the scattering properties. The enhanced light scattering is also responsible to the higher IPCE obtained for pine tree HBS in the wavelength range of 500–650 nm. By sensitization with CdS/CdSe QDs, the devices yielded an overall efficiency of ~3 %, which was higher than that of ZnO nanowire arrays due to increased QDs loading and enhanced light scattering by the 3D geometry. It was also noted that the doping in

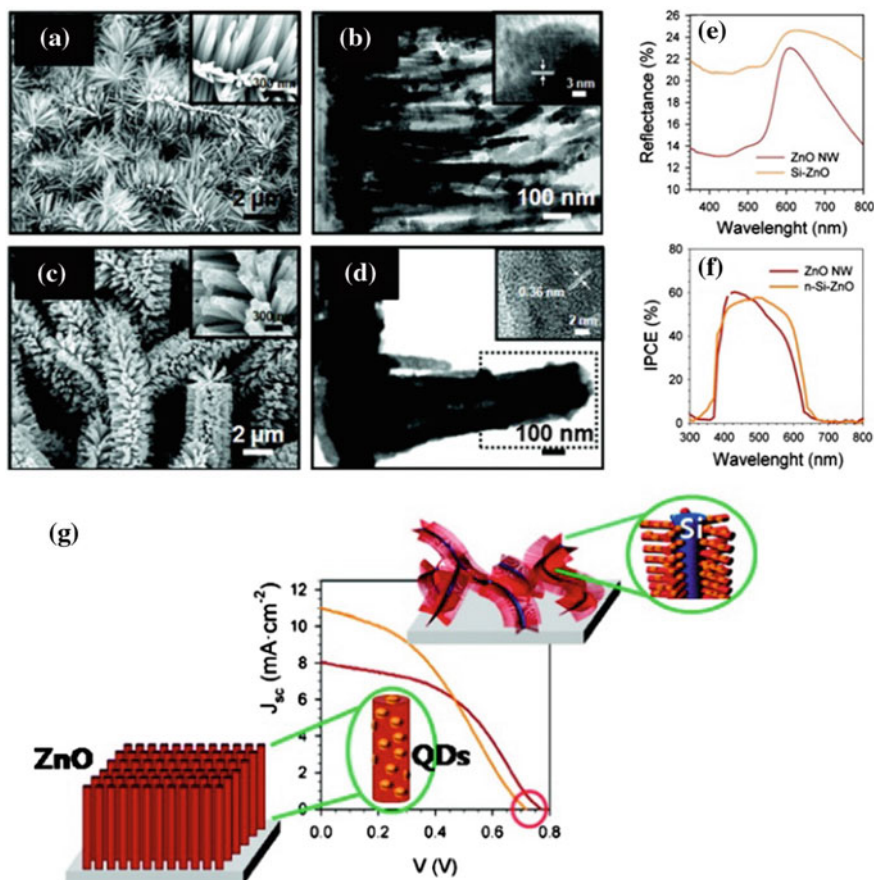


Fig. 15 a and c SEM images of pure and QDs-sensitized Si/ZnO hierarchical structure, respectively; b and d, corresponding TEM images; e diffused reflectance spectra and f IPCE spectra of Si/ZnO hierarchical anode based QDSCs; g J-V performance of conventional ZnO nanowire array and Si/ZnO hierarchical anode-based QDSCs compared with corresponding schematic anode structure (Sudhagar et al. [70] ©Reprint permission from ACS Publishers)

the Si backbone nanowire played an important role in the performance: the ZnO NR had a J_{sc} of 8.0 mA/cm² and efficiency of 2.7 %, whereas the 3-D pine tree QDSC resulted in J_{sc} of 11.00 mA/cm² and efficiency of 3.00 % (Fig. 15g). It is indicated, pine tree structures have the additional advantage of the fast electron transport through n-Si NWs. More importantly, we demonstrated that it is possible to obtain higher V_{oc} QDSCs with an appropriate treatment of the recombination process, highlighting the fact that QDSCs have to be rethought, separately of DSCs, to optimize their performance.

4.3 Inverse Opal Architecture Photoanodes

The disordered geometrical structure of conventional nanoparticle-based photoanode is often limiting the performance of the sensitized-type solar cells due to interfacial interference for electron transport. Mainly, trap-limited diffusion process in randomly connected networks can be affected by recombination with the oxidizing species in the electrolyte during trapping process. Therefore, designing the anode frameworks with highly interconnected morphology is a promising approach in achieving superior charge transport and high penetration of both sensitizers and redox couples. In this context, a nanostructure which contains bottom-up 3D host–passivation–guest (H–P–G) electrode has been realized as promising candidate in DSSCs [129, 130]. Since, 3-D H-P-G electrode offer good structural control in the electron extraction and the recombination dynamics, this new type of H-P-G electrode has significantly promoted the photocurrent, fill factor, and most importantly the photovoltage of DSSCs [131].

The H-P-G electrode is basically developed by micromolding in inverse opals (IO) structures using colloidal crystals [132]. It is well reported that inverse opal TiO_2 has large interconnected pores that lead to a better infiltration, also it exhibits a photonic bandgap (photonic crystal), which depends on the filling fraction of TiO_2 in the inverse opal structure. The preparation procedure of IO electrodes has been demonstrated in two stages. First, the host layer is self-assembled on TCO substrates, subsequently secondary coating of guest (TiO_2) layer coated on the host. The preparation methods of 3-D TiO_2 IO electrodes were schematically explained in the Fig. 16a. The host layer may be assembled by either chemical or physical technique. It is widely demonstrated that the polymer microspheres are utilized as host layer (polystyrene, co-polymers, etc.) since it is easily removable without altering the final TiO_2 morphology. Figure 16a shows the deposition of TiO_2 layer by chemical method, which support for large-scale fabrication at low cost. Besides, it is difficult to control the thickness of the TiO_2 layer in this approach. The undesired thick TiO_2 coating could clog the mesoscopic pores of the host layer, which would inhibit sensitization and electrolyte infiltration. This can be overcome by physical coating like “atomic layer deposition” (ALD), where the thin guest layer can be conformably coated on the entire polymer microspheres (Fig. 16b) without clogging the pore structure [129, 133–135]. Finally, polymer beads were removed (Fig. 16c) by high temperature annealing or with solvents at room temperature, we obtained a 3D host backbone that is well connected to the underlying TCO substrate. The resultant direct electronic connection with TCO facilitates the charge extraction throughout the interconnected 3D H–P–G electrode. The IO photonic crystal are playing crucial roles in DSSCs as a (a) dielectric mirror for wavelengths corresponding to the stop band and (b) medium for enhancing light absorption on the long-wavelength side of the stop band [136, 137]. The advantages of light interaction in these structures ultimately enhance the backscattering of the device through localization of heavy photons near the edges of a photonic gap. This scattered light increases the probability of light absorption

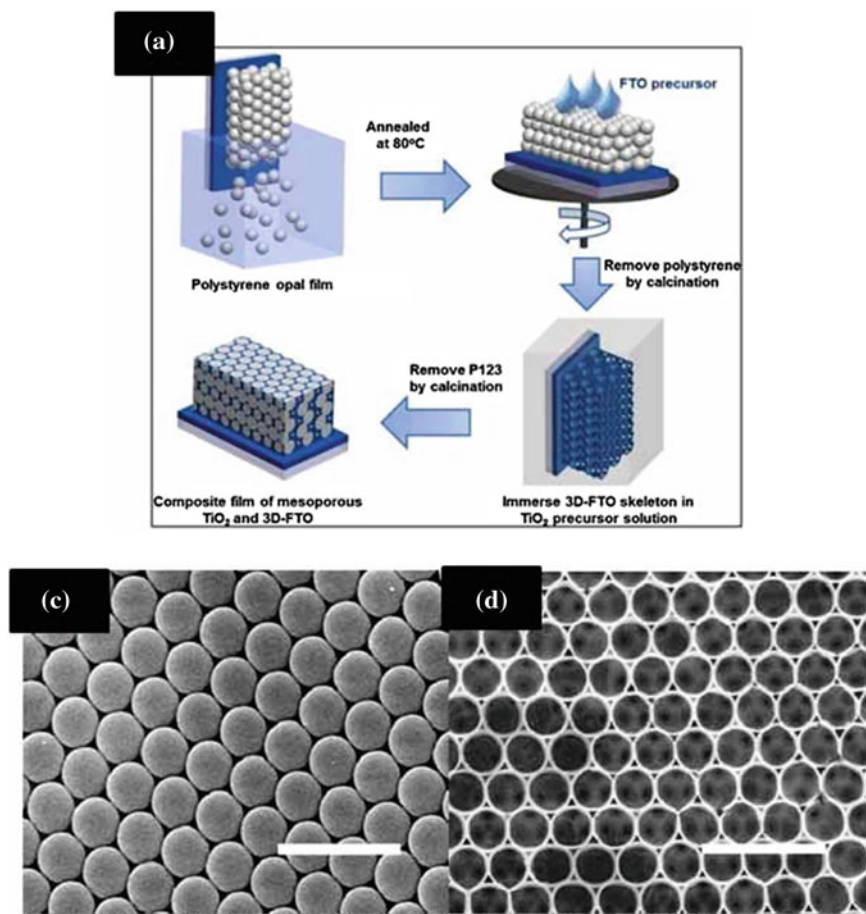


Fig. 16 a Schematic illustration of the forming 3-D TiO_2 Inverse Opal Structures by chemical solution method; SEM images of (c) polystyrene beads (host) and (d) TiO_2 inverse opal (after removing polystyrene beads); (Reprint permission from Science Direct, [142] and ACS publisher

especially in the red part of the solar spectrum. Wide range of IO-based photanodes were exemplified in DSSCs as a (a) effective scaffold for high sensitizer loading [138] (b) scattering layer [139, 140] (c) window layer for more light photon harvesting [141], and (d) high electron-collection 3-D conductive grid [142]. Among many characteristics of IO, particularly opal size (diameter) [133, 143] and thickness of the electrode [131, 138, 144] has influencing the device performance of DSSCs.

The QDSCs with IO electrodes has been well demonstrated by Prof. Toyoda group. The influence of the QDs deposition time at IO surface was studied in detail [145]. Diaguna et al. studied the influence of opal diameter on photovoltaic performance [146]. The J-V performance of two different TiO_2 inverse opal

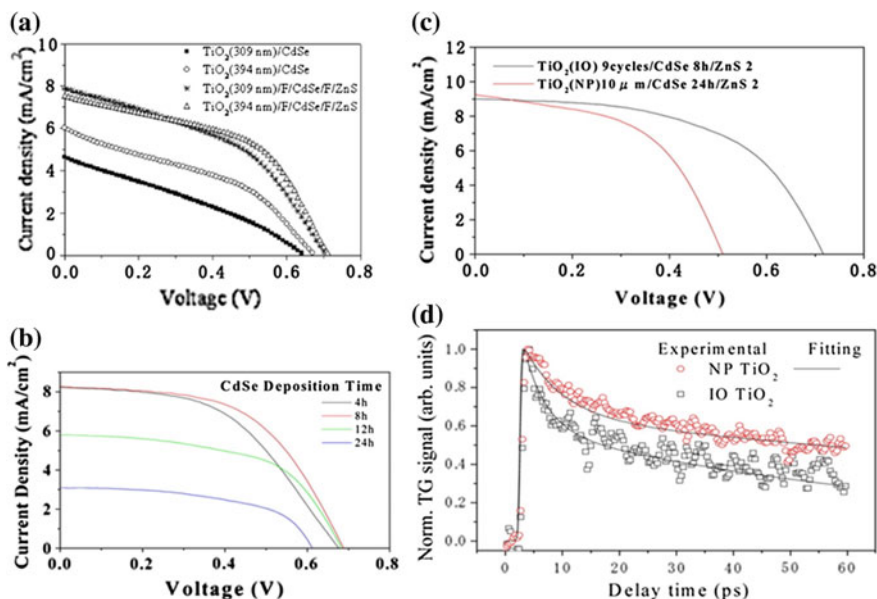


Fig. 17 **a** J-V characteristic of two different TiO₂ inverse opal electrodes made from latex template with diameters of 309 and 394 nm [146]; **b** Photocurrent density–photovoltage characteristics of CdSe QD-sensitized inverse opal TiO₂ solar cells with different adsorption times [145]; **c** Photocurrent density–photovoltage characteristics of CdSe QD-sensitized inverse opal TiO₂ and nanoparticulate TiO₂ solar cells with the same electrode thickness [145]; **d** Time dependence of the TG signal intensity of CdSe QD-sensitized inverse opal (IO) and nanoparticulate (NP) TiO₂ solar cells [145] (Reprint permission from IOP publishers, [146] and RSC Publishers [145])

electrodes made from latex template with diameters of 309 and 394 nm was tested (Fig. 17a). The wide pore size of opal 394 nm results slightly higher efficiency 2.7 % than the smaller pore size opal-based cell (2.4 %) [146]. Further, Toyoda et al. explored how the wide pore nature of IO supports the efficient QDs coating [145]. Figure 17b shows the JV performance of IO-based QDSSCs with different amount of QDs loading. From Fig. 17b it clearly understands that 8 h chemical bath deposited CdSe QDs coating performed higher than that of 4 h QDs coating. The former QDs coating result 3.1 % of PCE with $J_{sc} = 8.3 \text{ mA cm}^{-2}$, $V_{oc} = 0.69 \text{ V}$ and $FF = 0.57$. In the case of later one (4 h CdSe QD coating) results 2.8 % of PCE with $J_{sc} = 8.2 \text{ mA cm}^{-2}$, $V_{oc} = 0.68 \text{ V}$ and $FF = 0.54$. Further enhancing the QDs deposition to 24 h, the PCE was found to be reduced to 1.0 % ($J_{sc} = 3.1 \text{ mA cm}^{-2}$, $V_{oc} = 0.61 \text{ V}$ and $FF = 0.55$) due to pore blockage, which severely affect the electrolyte penetration. Thus, result poor hole scavenging at QDs/IO interfaces, and lower the V_{oc} and J_{sc} [145]. In order to understand the feasibility of IO electrode in QDSCs, the typical PV performance of IO is compared with NP electrode in Fig. 17c. Both IO and NP electrode thickness is about 9 μm. The IO-based QDSSC showed a higher efficiency (3.5 %) than that of the

nanoparticulate-based QDSSC (2.4 %) due to the higher V_{oc} , although the amount of CdSe QDs in the inverse opal case might be a half of that in the nanoparticulate case due to the difference of surface area. The higher V_{oc} in the IO QDSSCs was ascribed to the larger fraction of electron injection to the TiO_2 resulting in a higher quasi Fermi level, detected with ultrafast optical measurements, Fig. 17d. In addition to the above comparative results, Samadpour et al. also compared the performance of IO-based QDSSCs along with variety of nanostructured electrodes (nanotube, nanofiber, and nanoparticulate) [71]. They suggested that choosing the semiconductor deposition strategy (CBD or SILAR) is more important where the pore blockage takes a key role which influences the efficiency of QDSSCs.

5 Hole Transporting Material

Concerning the hole transporting material, it is a major difference with liquid DSSCs as many of the most employed semiconductors for light harvesting are not stable in solutions with the conventional I^-/I_3^- redox couple [7]. Stability problems could be solved by the use of Co redox couples, but the photocurrents obtained were relatively low [40, 60, 76]. The other approximation used to solve this issue was the coating of the semiconductor QDs with a protecting layer of amorphous TiO_2 [147]. However, obtained photocurrent was not much appreciable. In order to solve these issues, the most common redox couple employed for QDSSCs is the polysulfide (S^{2-}/S_n^{2-}), generally in an aqueous solution [148]. Polysulfide redox helps in the stability of semiconductor light absorber in the liquid devices, it also allows high photocurrents (photocurrents as high as 22 mA/cm^2 has been recently reported for PbS/CdS QDSSCs [149]), but it introduces an additional problem of a bad charge transfer with the platinized counter electrodes [21] commonly used in DSSCs. As a consequence very bad fill factors, FF, are commonly reported with platinized electrodes and polysulfide redox, see for example, refs. [21, 146]. In order to replace this inconvenient Pt catalytic electrodes, the fourth aspect commented previously has been developed for polysulfide electrolyte. We will come back with this issue later.

There are three interesting aspects that is worthy to comment related with polysulfide redox electrolytes. The first one is related with a deceptive practice that unfortunately is reported in a relatively significant number of papers. One of the requirements that an electrolyte for sensitized solar cells has to fulfil is the stability during a complete charge extraction process. Reduced species of the redox couple are oxidized during the hole regeneration of the sensitizer. Oxidized species diffuse to the counter electrode where they are reduced again in a fully regenerative process. This is the case of aqueous polysulfide electrolyte, but it is not strange to find a paper where methanol is added as solvent. Methanol acts as a hole scavenger regenerating oxidized sensitizers, but it is not regenerated itself at the counter electrode, as the redox couples. As a consequence cells prepared with methanol in

the electrolyte increases artificially the photocurrents, but this effect disappears when the methanol is exhausted. Obviously, this electrolyte cannot be used in a solar cell that demands a long device lifetime.

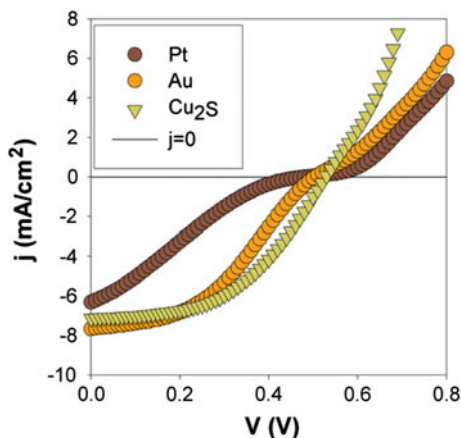
Related with this aspect, it is also important to work in the long-term stability of QDSSCs. There are very few reports in this issue, probably as the first aspects that the authors want to optimize is the efficiency as for most of the QDSSCs studied it lays significantly below than the efficiency reported for DSSCs. The main problem of liquid devices is the volatility of the electrolyte. It forces to use very sophisticated (and sometimes expensive) sealing processes in order to avoid electrolyte leakage. A common procedure systematically used in DSSCs is to employ ionic liquid, with significantly lower volatility than the standard solvents, as electrolytes. The reduced volatility eases the process of sealing that cheapens the cell at the same time that extends the device lifetime. The price of this improvement is a reduction in efficiency due to the increase in the diffusion of species in the electrolyte. A similar approximation has been developed for QDSSCs but using ionic liquids based on sulfide/polysulfide instead of the ionic liquids based on iodine employed on DSSCs [150]. Despite, further work is required to optimize the results sulfide/polysulfide ionic liquids could present promising results in terms of cell stability.

Nevertheless at this moment there is no optimum electrolyte for QDSSCs. Proof of this is the fact that the efficiencies obtained in liquid QDSSCs are no higher than those obtained in solid cells, while in the case of DSSCs the efficiencies of liquid cells is sensibly higher than solid ones. At least until the apparition of the cells using lead halide perovskite as light absorbing material, we will discuss this especial case in the Sect. 8. With the exception of perovskites the semiconductor providing the highest efficiency in all-solid sensitized devices is Sb_2S_3 , with an efficiency of 6.3 % [67]. The study of this material in solid configuration was approached for the first time by Larramona and co-workers [151] and independently by Messina et al. [152]. In the case of Larramona CuSCN , a wide band gap p-type semiconductor, was used as HTM, while in Messina's work they contacted directly Sb_2S_3 for hole extraction. Very encouraging results were reported later by the groups of Hodes, [49] and Hodes and Grätzel, [153] in this last one using spiro OMeTAD as HTM. But the higher results have been reported by the groups of Seok and Grätzel [68, 154] using conductive polymers as HTM that boosted the efficiency to unprecedented values, at that moment, values of 5–6 %, even higher than liquid QDSSCs.

6 Counter Electrode

The last consideration concerning polysulfide electrolyte is related with the counter electrode. We have already discussed that platinized counter electrodes are one of the causes of poor FF obtained for QDSSCs with polysulfide electrolyte [21, 146]. This problematic cause was already discussed at the beginning of the 1980s by

Fig. 18 Effect of counter electrode material on the QDSSC performance. The effect is especially evident in the FF (Reprinted permission with Giménez et al. [24])



Hodes et al. [155] suggesting PbS, CoS, and Cu_2S as alternative counter electrodes for a good charge transfer with aqueous polysulfide. All three counter electrode materials have been investigated in QDSSCs. PbS counter electrodes increases significantly the cell performance of QDSSCs with polysulfide electrolyte, especially by the increase of FF and photocurrent [57]. PbS has been also studied in combination with carbon black [156]. Carbon foam was also checked [157]. Cu_2S , CoS, and combination of both materials have been also employed in the development of QDSSCs [158]. But probably Cu_2S has been the material most used in the preparation of efficient counter electrodes for polysulfide electrolyte and the record cells with polysulfide, 6.36 % efficiency with $\text{CdSe}_x\text{Te}_{1-x}$ colloidal quantum dots, [38] has been prepared using this material as the base of the counter electrode. This material presents higher performance than platinized and Au counter electrodes, see Fig. 18. Generally, it is prepared from a thin foil [24]. But in this format the sealing of active electrode and counter electrode becomes difficult. To solve this inconvenience Cu_2S pastes that can be deposited on transparent conductive oxide substrates has been developed [159]. An interesting alternative is the use of Cu_2S -reduced graphene oxide composite [160]. Briefly, graphene oxide is reduced by adding Cu ions in its structure, see Fig. 19. Cu_2S is finally formed with the help of sulfur atoms (just by using a polysulfide solution). Finally, a powder is obtained and properly treated can be deposited by doctor blade in the conductive substrate. This counter electrode has been used in the preparation of record cell in that moment with 5.4 % efficiency [161] (Fig. 20).

7 Recombination and Surface States

In this sense, Sb_2S_3 exhibits an interesting potentiality for the development of efficient QDSSCs, but in order to improve the obtained results, it is needed to reduce the recombination in photovoltaic devices using this material as light

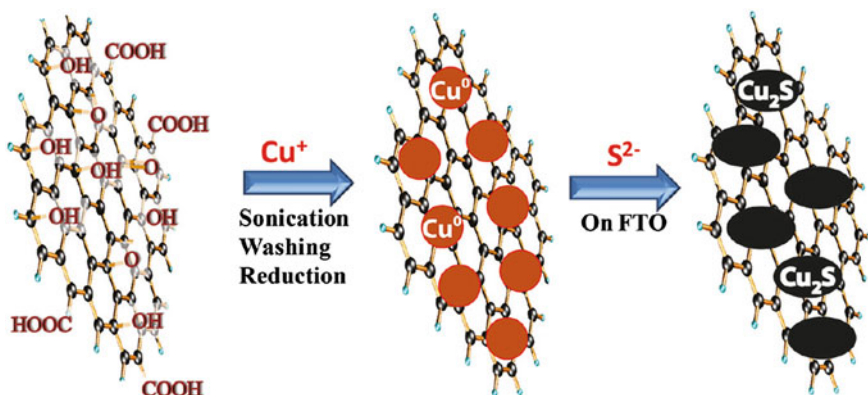


Fig. 19 Scheme of the preparation of reduced graphene oxide with Cu₂S nanocomposite for applications as counter electrode material in QDSSCs (Reprinted permission with Radich et al. [160])

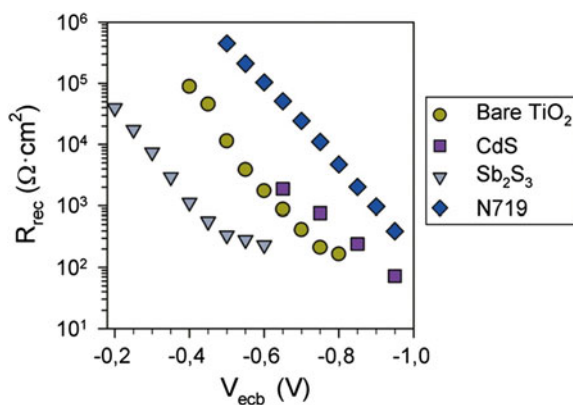


Fig. 20 Recombination resistance of bare mesoporous electrode of TiO₂ and three sensitized TiO₂ electrodes. Electrodes have been sensitized with the molecular dye N719 and with two inorganic semiconductors CdS and Sb₂S₃. Recombination resistance has been measured with impedance spectroscopy in three electrode configuration with liquid electrolyte. Recombination resistance is inversely proportional to the recombination rate and it is plotted as function of the equivalent conduction band potential, V_{ecb} , where the shift of the conduction band [188] of the different electrodes has been removed (Reprinted permission with Boix et al. [189])

absorber. This fact highlights the last of the five aspect in which QDSSCs shows sensible differences with DSSCs. In Fig. 19 recombination resistance, R_{rec} , of TiO₂ electrodes bare or sensitized with different materials is depicted. Note that the recombination is reduced, in comparison with bare TiO₂, when the electrode is sensitized with the molecular dye N719, as the molecule acts as a blocking layer for the recombination of electrons in TiO₂. In contrast, only a slight decrease in

recombination (slight increase in R_{rec}) is observed when CdS is used as sensitizer. But, in the case of Sb_2S_3 recombination is even enhanced in comparison with bare electrode. This fact indicates that the inorganic sensitizer itself has an active role in recombination process, in other word the sensitizer introduces active recombination site where photoinjected electron in the TiO_2 find a pathway for recombination. Here a clear difference with DSSC is highlighted, while molecular dyes only presents the HOMO and LUMO levels for shelter electrons, in the case of QDs or inorganic semiconductors, surface states could play an important role in the QDSSCs performance [7]. In fact the main effect of the well-known ZnS treatment that enhances significantly QDSSCs in many cases, [10, 24, 34] is to passivate the surface states of the inorganic sensitizer [162]. Thus, the recombination though the sensitizer in QDSSCs has to be reduced in order to improve the photovoltaic conversion efficiency, passivation treatments of TiO_2 surface [163], or of the light absorbing material itself [164, 165] have shown a tremendous effect in the cell performance, but further analysis in this direction is needed to continue the optimization of QDSSCs. On the other hand, each kind of inorganic semiconductor could require a different passivation process in terms of stability and efficiency of the semiconductor layer.

Finally as introduction for the next section, it has to be highlighted that in addition one of the effective approaches to control the recombination rate in QD-sensitized solar cells (QDSSCs) is to densely cover the QDs on mesoporous-nanostructured electrodes [10] without naked sites, that directly block the physical contact between electrolyte and TiO_2 [166, 167] In this configuration, semiconductor sensitizer layer is acting as a barrier between electrons in the TiO_2 and accepting species in the electrolyte hindering this recombination path way, but recombination though sensitizer semiconductor is still possible as it has been previously commented. Taking into account this consideration, the procedure in with electrodes sensitized also plays an important role in the recombination of QDSSCs [71].

8 The Perovskite Revolution

Recently, a new type of photovoltaic cells with organometallic halide perovskites as light harvester materials have burst onto the scene gaining great attention in the scientific community. It is due mainly because a rapid succession of occurrences of record devices in a short-time period, which it is now reaching above of 14 % of certified efficiency, [168] and even further increase has been announced. Here, we briefly review the most striking results in the current hottest topic on photovoltaics.

8.1 Structure, Chemical Composition, and Optoelectronic Properties of Halogenated Perovskites

The halogenated hybrid perovskites have been previously studied as semiconducting materials processable in solution at low temperature for thin-film field-effect transistors, where they have shown to have a high mobility of carriers compared with organic materials [169]. Hybrid perovskites of type ABX_3 ($A = CH_3NH_3^+$, $B = Pb^{2+}$, $X = Cl^-, Br^-, I^-$) used in the newly developed photovoltaic devices are formed by inorganic layers of lead halide corner-sharing octahedrals interpenetrated by an alkylammonium cation network where the size of the organic cation plays an important role to define the final type of perovskite structure formed, Fig. 21.

The most used cations in the cells reported to date were methylammonium and lead (II) for the positions A and B, respectively. $(CH_3NH_3)PbI_3$ compound has a direct bandgap of 1.51 eV determined experimentally [170] and theoretically [171]. Also, this hybrid organometal halide perovskite has a high absorption coefficient compared to the N719 dye [172]. The work function studied by photoelectron spectroscopy of spin-coated polycrystalline films showed valence-band levels of $(CH_3NH_3)PbI_3$ and $(CH_3NH_3)PbBr_3$ at -5.44 and -5.38 eV versus the vacuum level, respectively and the conduction band levels calculated from the optical absorption edges are at -4.0 and -3.36 . Therefore, these profiles mean that electron injection to the TiO_2 conduction band is favored. Figure 22 summarizes the main optoelectronic properties of $(CH_3NH_3)PbI_3$.

8.2 Construction of Solid-State Devices Using Wet Methods

Perovskites have been used as light harvester since 2009 when Miyasaka et al. [173] reported that these materials could be an alternative to binary chalcogenide based on QDSSCs, reaching an efficiency of 3.8 %, Fig. 23. An interesting aspect of the manufacture of these devices is that the active material is solution processable using a stoichiometric solution of $(CH_3NH_3)I$ and PbI_2 at room temperature and without employ vacuum techniques. However, the liquid electrolyte used as hole transport layer rapidly degrades the active material of sensitized cell. Approximately 2 years later, a work from Park and collaborators developed a cell which had twice the efficiency of Miyasaka cell due mainly to the use of more concentrated perovskite precursor solutions [172]. However, the cell was also deteriorated rapidly by the liquid electrolyte.

The breakthrough in efficiency (9.7 %) and stability (> 500 h) was done by the same group in 2012 using a solid electrolyte, the spiro-MeOTAD, instead of liquid electrolyte, Fig. 24 [170]. At the same time, devices whose active layer is also

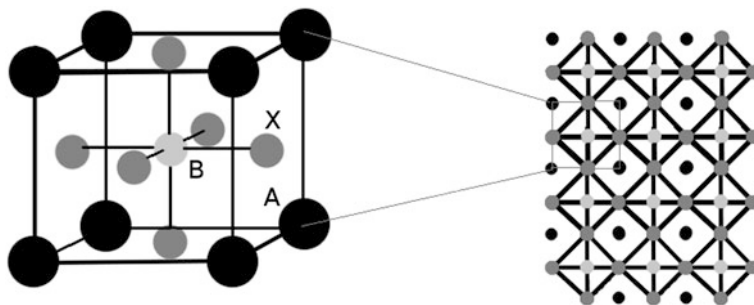


Fig. 21 3D structure for ABX_3 type perovskites

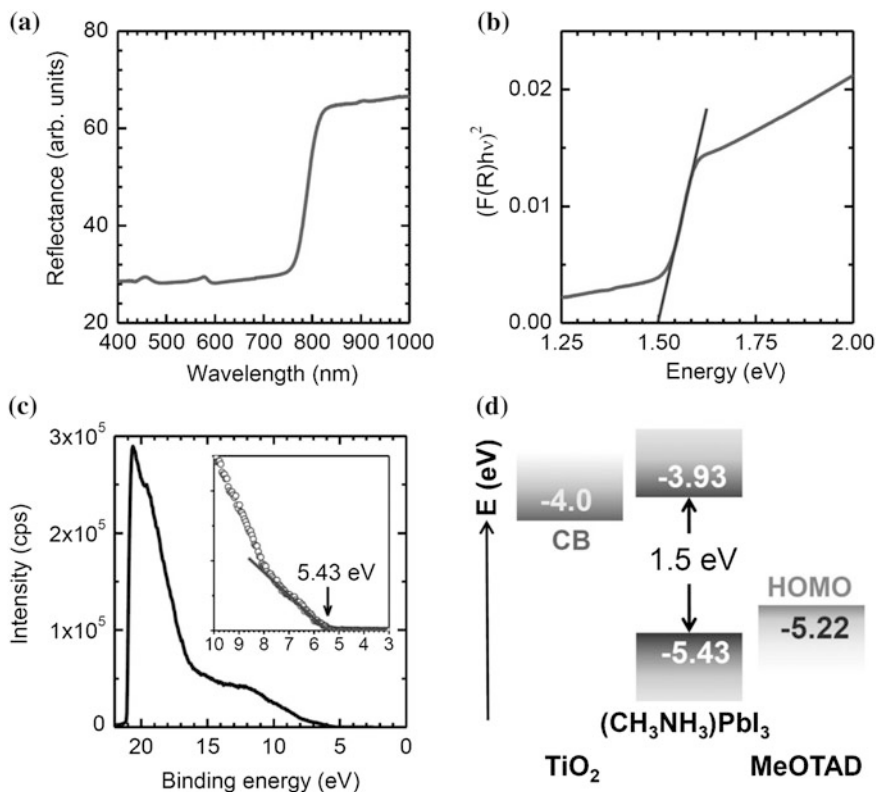


Fig. 22 Diffuse reflectance and UPS spectra for $(CH_3NH_3)PbI_3$ perovskite sensitizer. **a** Diffuse reflectance spectrum of the $(CH_3NH_3)PbI_3$ -sensitized TiO_2 film. **b** Transformed Kubelka-Munk spectrum of the $(CH_3NH_3)PbI_3$ -sensitized TiO_2 film. **c** UPS spectrum of the $(CH_3NH_3)PbI_3$ -sensitized TiO_2 film. **d** Schematic energy level diagram of TiO_2 , $(CH_3NH_3)PbI_3$, and spiro-MeOTAD (Reprinted permission with Kim et al. [170])

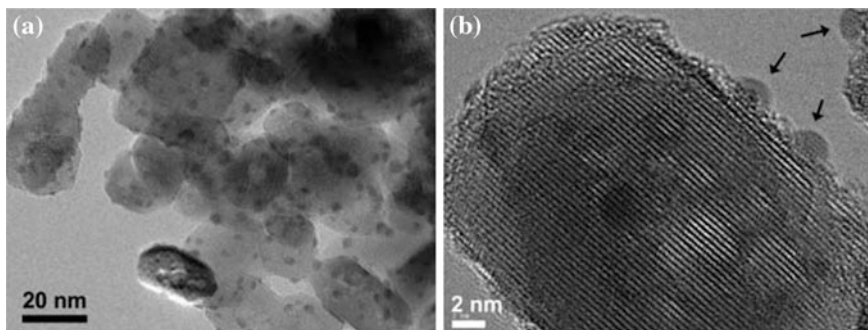


Fig. 23 TEM micrographs of (a) wide view of (CH₃NH₃)PbI₃ deposited TiO₂ (b) magnified image of (CH₃NH₃)PbI₃ deposited TiO₂. (Reprinted permission with Im et al. [172])

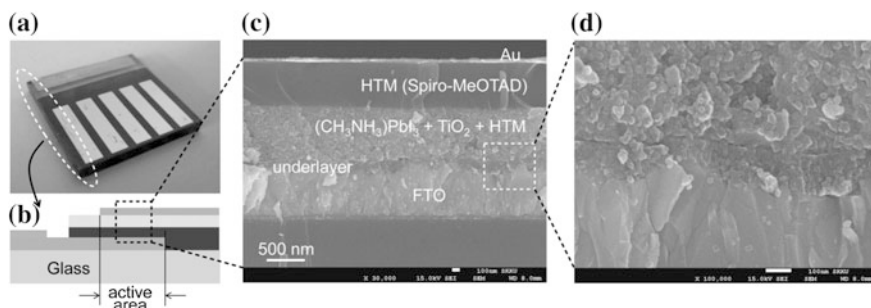


Fig. 24 Solid-state device and its cross-sectional mesostructure. **a** Real solid-state device. **b** Cross-sectional structure of the device. **c** Cross-sectional SEM image of the device. **d** Active layer-underlayer-FTO interfacial junction structure (Reprinted permission with Kim et al. [170])

deposited by spin-coating but the formulation of the perovskite incorporates a halogens mixture (CH₃NH₃)PbI₂Cl, and the scaffold material is Al₂O₃ reached PCE profiles of 10.9 % [174]. The perovskite is not able to inject electrons in the Al₂O₃-mesostructured scaffold but the HTM layer, the spiro-MeOTAD, compensates the situation injecting and transporting holes efficiently to the cathode. Etgar et al. went one step further publishing a work where the HTM layer of the cell is removed and the efficiency of the cell remains above 5 % using TiO₂ as scaffold for the perovskite [175]. The two last discoveries raise the question if these cells should be considered classic sensitized dye cells. But the last works published in such devices to early and mid-2013, are more focus in increasing the cell efficiency that in attempting to elucidate the mechanisms of storage, transportation and injection of electrons and holes. High efficiency has been also obtained by using polymeric HTM, [176] different morphologies of mesostructured layer, [177] perovskites with a mixture of halogens, [178, 179] and an impressive manufacturing technique employing sintering temperatures below 150 °C and efficiencies

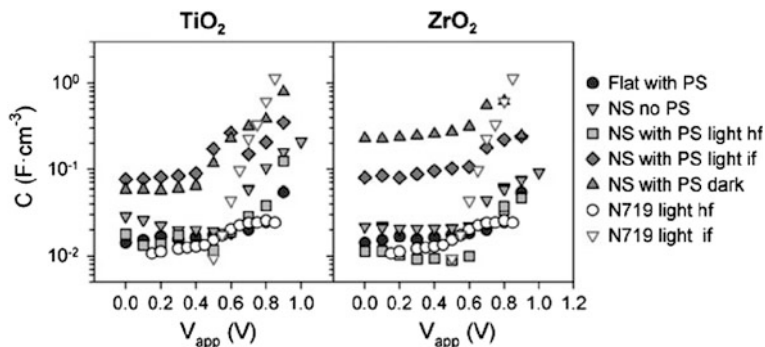


Fig. 25 Left graph plots capacitance of: flat sample with perovskite (PS); blank NS TiO₂ (0.35 μm thickness) with no PS; NS TiO₂ (0.55 μm thickness) with PS extracted from measurement under dark and under 1 sun illumination (light) conditions; and all-solid DSSC (2.2 μm thickness) with N719 as dye and spiro-MeOTAD as HTM. Right graph plots capacitance of flat sample with perovskite (PS); blank NS ZrO₂ (0.39 μm thickness) with no PS; NS TiO₂ (0.36 μm thickness) with PS extracted from measurement under dark and under 1 sun illumination (light) conditions; and all-solid DSSC (2.2 μm thickness) with N719 as dye and spiro-MeOTAD as HTM. Capacitance has been normalized to the electrode volume. Capacitance for both graphs has been extracted by fitting the impedance spectroscopy spectra from the intermediate frequency (*if*) region if nothing else is indicated. In some cases capacitance has been extracted from the high frequency (*hf*) region as it is indicated in the legend (Reprinted permission with Kim et al. [182])

of 12.3 % [180]. In addition impressive V_{oc} of 1.3 V has been also reported for (CH₃NH₃)PbBr₃ [181].

Finally, a recent study [182] focusing on the analysis of capacitances in perovskite solar cells using photoanodes with both TiO₂ and ZrO₂ mesoporous photoanodes, have shown a similar behavior despite the significant differences between both (electrons cannot be injected from (CH₃NH₃)PbI₃ into ZrO₂ as in the case of Al₂O₃). In both cases a capacitance that can be attributed to the perovskite has been detected (Blue triangles and green diamonds in Fig. 25). This capacitance indicates that charge accumulation is occurring in the perovskite itself in contrast with conventional all-solid DSSC where the charge accumulation is produced in the TiO₂ after photoinjection (red inverted triangles in Fig. 25). This is, the first observation of charge accumulation in the light absorbing material for nano-structured solar cells, indicating that it constitutes a new kind of photovoltaic device, halfway between sensitized and thin-film solar cell for NS TiO₂ and a thin-film solar cell with ZrO₂ scaffold for NS ZrO₂.

In summary, perovskite (CH₃NH₃)PbI₃-sensitized or mesoscopic solid-state solar cells using different HTMs (polymeric or molecular materials), scaffolds and halides are a promising type of solar cells to be converted in real-life manufactured devices in short time. However, the fast succession of record devices prepared last year, Fig. 26, is not being balanced with a full understanding of these cells work, and more studies in the theoretical plane are needed.

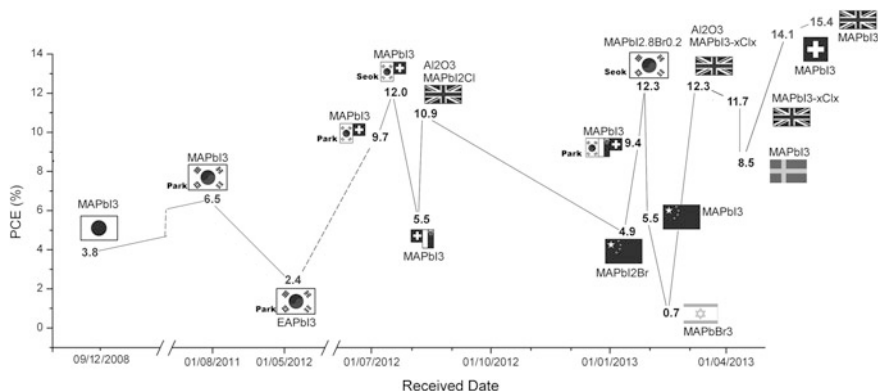


Fig. 26 Time evolution of published papers of hybrid perovskite solar cells (received date by the journal) versus PCE reported profiles of record cells; (red) liquid electrolyte (black), solid electrolyte

8.3 Conclusions

Despite the limited efficiencies obtained in the early stages of the study of QDSSCs, the potentialities of semiconductor thin layer or quantum dots has impelled the research on this devices in the last few years. We noted that the problems of such devices are different in many respects to that happening in DSSC, while both types of solar cells work according to the same principles. In QDSSC, the sensitizer material can be prepared in several ways affecting the final device performance. Photoanode nanostructure, hole transporting material, counter electrode, and recombination processes (affected by semiconductor trapping states) have to be optimized in order to enhance the reported efficiencies. As a result of the intense work on QDSSCs a real breakthrough, with organometallic halide perovskites, has occurred very recently. Solar cells with efficiencies as high as 15 % are reported, and it looks that further increase will be attained soon. In addition to the impressive efficiencies one of the strongest points of these new cells is that they can be prepared from solution techniques, as the once developed for QDSSCs, and consequently the production cost of the photovoltaic device can be dramatically reduced.

References

1. Tyler Miller Jr G (2007) Living in the environment. Thomson Brooks/Cole, London
2. United Nations Framework Convention on Climate Change (Text) (1992) (UNEP/WMO, Climate Change Secretariat, Geneva, 1992)
3. Barber J (2009) Photosynthetic energy conversion: natural and artificial. Chem Soc Rev 38(1):185–196

4. Bisquert J, Cahen D, Hodes G, Rühle S, Zaban A (2004) Physical chemical principles of photovoltaic conversion with nanoparticulate, mesoporous dye-sensitized solar cells. *J Phys Chem B* 108:8106–8118
5. O' Regan B, Grätzel M (1991) A low-cost high-efficiency solar cell based on dye-sensitized colloidal TiO₂ films. *Nature* 353:737–740
6. Peter LM (2011) The Grätzel cell: where next? *J Phys Chem Lett* 2:1861–1867
7. Hodes G (2008) Comparison of dye- and semiconductor-sensitized porous nanocrystalline liquid junction solar cells. *J Phys Chem C* 112(46):17778–17787
8. Robel I, Subramanian V, Kuno M, Kamat PV (2006) Quantum dot solar cells. harvesting light energy with CdSe nanocrystals molecularly linked to mesoscopic TiO₂ films. *J Am Chem Soc* 128:2385–2393
9. Zaban A, Micic OI, Gregg BA, Nozik AJ (1998) Photosensitization of nanoporous TiO₂ electrodes with InP quantum dots. *Langmuir* 14(12):3153–3156
10. Mora-Seró I, Giménez S, Fabregat-Santiago F, Gómez R, Shen Q, Toyoda T, Bisquert J (2009) Recombination in quantum dot sensitized solar cells. *Acc Chem Res* 42(11):1848–1857
11. Leschkies SK, Divakar R, Basu J, Enache-Pommer E, Boercker JE, Carter CB, Kortshagen UR, Norris DJ, Aydil ES (2007) Photosensitization of ZnO nanowires with CdSe quantum dots for photovoltaic devices. *Nano Lett* 7(6):1793–1798
12. Hossain A, Yang GW, Parameswaran M, Jennings JR, Wang Q (2010) Mesoporous SnO₂ spheres synthesized by electrochemical anodization and their application in CdSe-Sensitized Solar Cells. *J Phys Chem C* 114(49):21878–21884
13. Hossain MA, Jennings JR, Koh ZY, Wang Q (2011) Carrier generation and collection in CdS/CdSe-sensitized SnO₂ solar cells exhibiting unprecedented photocurrent densities. *ACS Nano* 5(4):3172–3181
14. Hossain MA, Koh ZY, Wang Q (2012) PbS/CdS-sensitized mesoscopic SnO₂ solar cells for enhanced infrared light harnessing. *Phys Chem Chem Phys* 14(20):7367–7374
15. Samadpour M, Giménez S, Boix PP, Shen Q, Calvo ME, Taghavinia N, zad AI, Toyoda T, Míguez H, Mora-Seró I (2012) Effect of nanostructured electrode architecture and semiconductor deposition strategy on the photovoltaic performance of quantum dot sensitized solar cells. *Electrochimica Acta* 75(0):139–147
16. Giménez S, Xu X, Lana-Villarreal T, Gómez R, Agouram S, Muñoz-Sanjosé V, Mora-Seró I (2010) Determination of limiting factors of photovoltaic efficiency in quantum dot sensitized solar cells: correlation between cell performance and structural properties. *J Appl Phys* 108:064310
17. Vogel R, Hoyer P, Weller H (1994) Quantum-sized Pbs, Cds, Ag₂s, Sb₂s₃, and Bi₂s₃ particles as sensitizers for various nanoporous wide-bandgap semiconductors. *J Phys Chem* 98(12):3183–3188
18. Lin SC, Lee YL, Chang CH, Shen YJ, Yang YM (2007) Quantum-dot-sensitized solar cells: Assembly of CdS-quantum-dots coupling techniques of self-assembled monolayer and chemical bath deposition. *Appl Phys Lett* 90(14)
19. Yu XY, Liao JY, Qiu KQ, Kuang DB, Su CY (2011) Dynamic study of highly efficient CdS/CdSe quantum dot-sensitized solar cells fabricated by electrodeposition. *ACS Nano* 5(12):9494–9500
20. Hu HW, Ding JN, Zhang S, Li Y, Bai L, Yuan NY (2013) Photodeposition of Ag₂S on TiO₂ nanorod arrays for quantum dot-sensitized solar cells. *Nanoscale Res Lett* 8
21. Mora-Sero I, Gimenez S, Moehl T, Fabregat-Santiago F, Lana-Villarreal T, Gomez R, Bisquert J (2008) Factors determining the photovoltaic performance of a CdSe quantum dot sensitized solar cell: the role of the linker molecule and of the counter electrode. *Nanotechnology* 19(42)
22. Guijarro N, Lana-Villarreal T, Mora-Sero I, Bisquert J, Gomez R (2009) CdSe quantum dot-sensitized TiO₂ electrodes: effect of quantum dot coverage and mode of attachment. *J Phys Chem C* 113(10):4208–4214

23. Watson DF (2010) Linker-assisted assembly and interfacial electron-transfer reactivity of quantum dot-substrate architectures. *J Phys Chem Lett* 1:2299–2309
24. Giménez S, Mora-Seró I, Macor L, Guijarro N, Lana-Villarreal T, Gómez R, Diguna LJ, Shen Q, Toyoda T, Bisquert J (2009) Improving the performance of colloidal quantum dot sensitized solar cells. *Nanotechnology* 20:295204
25. Im SH, Lee YH, Seok SI, Kim SW, Kim SW (2010) Quantum-dot-sensitized solar cells fabricated by the combined process of the direct attachment of colloidal CdSe quantum dots having a ZnS glue layer and spray pyrolysis deposition. *Langmuir* 26(23):18576–18580
26. Zhu GA, Lv TA, Pan LK, Sun Z, Sun CQ (2011) All spray pyrolysis deposited CdS sensitized ZnO films for quantum dot-sensitized solar cells. *J Alloy Compd* 509(2):362–365
27. Benehkoal NP, Gonzalez-Pedro V, Boix PP, Chavhan S, Tena-Zaera R, Demopoulos GP, Mora-Sero I (2012) Colloidal PbS and PbSeS quantum dot sensitized solar cells prepared by electrophoretic deposition. *J Phys Chem C* 116(31):16391–16397
28. Salant A, Shalom M, Hod I, Faust A, Zaban A, Banin U (2010) Quantum dot sensitized solar cells with improved efficiency prepared using electrophoretic deposition. *ACS Nano* 4(10):5962–5968
29. Salant A, Shalom M, Tachan Z, Buhbut S, Zaban A, Banin U (2012) Quantum rod-sensitized solar cell: nanocrystal shape effect on the photovoltaic properties. *Nano Lett* 12(4):2095–2100
30. Santra PK, Kamat PV (2012) Tandem-layered quantum dot solar cells: tuning the photovoltaic response with luminescent ternary cadmium Chalcogenides. *J Am Chem Soc* 135(2):877–885
31. Lin S-C, Lee Y-L, Chang C-H, Shen Y-J, Yang Y-M (2007) Quantum-dot-sensitized solar cells: assembly of CdS-quantum-dots coupling techniques of self-assembled monolayer and chemical bath deposition. *Appl Phys Lett* 90:143517
32. Lee Y-L, Huang B-M, Chien H-T (2008) Highly efficient CdSe-Sensitized TiO₂ Photoelectrode for quantum-dot-sensitized solar cell applications. *Chem Mater* 20(22):6903–6905
33. Martínez-Ferrero E, Mora-Seró I, Alberoa J, Giménez S, Bisquert J, Palomares E (2010) Charge transfer kinetics in CdSe quantum dot sensitized solar cells. *Phys Chem Chem Phys* 12:2819–2821
34. Shen Q, Kobayashi J, Diguna LJ, Toyoda T (2003) Effect of ZnS coating on the photovoltaic properties of CdSe quantum dot-sensitized solar cells. *Journal of Appl Phys* 103(8)
35. Pernik DR, Tvrđy K, Radich JG, Kamat PV (2011) Tracking the adsorption and electron injection rates of CdSe quantum dots on TiO₂: linked versus direct attachment. *J Phys Chem C* 115(27):13511–13519
36. Pan Z, Zhang H, Cheng K, Hou Y, Hua J, Zhong X (2012) Highly efficient inverted type-I CdS/CdSe Core/Shell Structure QD-sensitized solar cells. *ACS Nano* 6(5):3982–3991
37. Zhang H, Cheng K, Hou YM, Fang Z, Pan ZX, Wu WJ, Hua JL, Zhong XH (2012) Efficient CdSe quantum dot-sensitized solar cells prepared by a postsynthesis assembly approach. *Chem Commun* 48(91):11235–11237
38. Pan Z, Zhao K, Wang J, Zhang H, Feng Y, Zhong X (2013) Near infrared absorption of Cd_{1-x}Te_x alloyed quantum dot sensitized solar cells with More than 6 % efficiency and high stability. *ACS Nano* 7(6):5215–5222
39. Alivisatos AP (1996) Semiconductor clusters, nanocrystals, and quantum dots. *Science* 271:933–937
40. Lee HJ, Yum J-H, Leventis HC, Zakeeruddin SM, Haque SA, Chen P, Seok SI, Grätzel M, Nazeeruddin MK (2008) cdse quantum dot-sensitized solar cells exceeding efficiency 1 % at full-sun intensity. *J Phys Chem C* 112:11600–11608
41. Liu L, Guo X, Li Y, Zhong X (2010) Bifunctional multidentate ligand modified highly stable water-soluble quantum dots. *Inorg Chem* 49(8):3768–3775

42. Jia S, Banerjee S, Herman IP (2008) Mechanism of the electrophoretic deposition of CdSe nanocrystal films: influence of the nanocrystal surface and charge. *J Phys Chem C* 112:162–171
43. Brown P, Kamat PV (2008) Quantum dot solar cells. Electrophoretic deposition of CdSe-C-60 composite films and capture of photogenerated electrons with nC(60) cluster shell. *J Am Chem Soc* 130(28):8890+
44. Mane RS, Lokhande CD (2000) Chemical deposition method for metal chalcogenide thin films. *Mater Chem Phys* 65(1):1–31
45. Chang CH, Lee YL (2007) Chemical bath deposition of CdS quantum dots onto mesoscopic TiO₂ films for application in quantum-dot-sensitized solar cells. *Appl Phys Lett* 91(5)
46. Jung SW, Kim JH, Kim H, Choi CJ, Ahn KS (2010) CdS quantum dots grown by in situ chemical bath deposition for quantum dot-sensitized solar cells. *J Appl Phys* 110(4)
47. Sudhagar P, Jung JH, Park S, Lee YG, Sathyamoorthy R, Kang YS, Ahn H (2009) The performance of coupled (CdS:CdSe) quantum dot-sensitized TiO₂ nanofibrous solar cells. *Electrochem Commun* 11(11):2220–2224
48. Lee YL, Huang BM, Chien HT (2008) Highly efficient CdSe-Sensitized TiO₂ photoelectrode for quantum-Dot-sensitized solar cell applications. *Chem Mater* 20(22):6903–6905
49. Itzhaik Y, Niiitsoo O, Page M, Hodes G (2009) Sb₂S₃-sensitized nanoporous TiO₂ solar cells. *J Phys Chem C* 113(11):4254–4256
50. Boix PP, Larramona G, Jacob A, Delatouche B, Mora-Sero I, Bisquert J (2012) Hole transport and recombination in all-solid Sb₂S₃-sensitized TiO₂ solar cells using CuSCN as hole transporter. *J Phys Chem C* 116(1):1579–1587
51. Maiti N, Im SH, Lim CS, Seok SI (2012) A chemical precursor for depositing Sb₂S₃ onto mesoporous TiO₂ layers in nonaqueous media and its application to solar cells. *Dalton Trans* 41(38):11569–11572
52. Gui EL, Kang AM, Pramana SS, Yantara N, Mathews N, Mhaisalkar S (2012) Effect of TiO₂ mesoporous layer and surface treatments in determining efficiencies in antimony sulfide-(Sb₂S₃) sensitized solar cells. *J Electrochem Soc* 159(3):B247–B250
53. Lan GY, Yang ZS, Lin YW, Lin ZH, Liao HY, Chang HT (2009) A simple strategy for improving the energy conversion of multilayered CdTe quantum dot-sensitized solar cells. *J Mater Chem* 19(16):2349–2355
54. Samadpour M, Zad AI, Taghavinia N, Molaei M (2011) A new structure to increase the photostability of CdTe quantum dot sensitized solar cells. *J Phys D Appl Phys* 44(4)
55. Yang ZS, Chang HT (2010) CdHgTe and CdTe quantum dot solar cells displaying an energy conversion efficiency exceeding 2 %. *Sol Energy Mater Sol Cells* 94(12):2046–2051
56. Yu XY, Lei BX, Kuang DB, Su CY (2011) Highly efficient CdTe/CdS quantum dot sensitized solar cells fabricated by a one-step linker assisted chemical bath deposition. *Chem Sci* 2(7):1396–1400
57. Tachan Z, Shalom M, Hod I, Rühle S, Tirosch S, Zaban A (2011) PbS as a highly catalytic counter electrode for polysulfide-based quantum dot solar cells. *J Phys Chem C* 115(13):6162–6166
58. Ju T, Graham RL, Zhai GM, Rodriguez YW, Breeze AJ, Yang LL, Alers GB, Carter SA (2010) High efficiency mesoporous titanium oxide PbS quantum dot solar cells at low temperature. *Appl Phys Lett* 97(4)
59. Lee H, Leventis HC, Moon SJ, Chen P, Ito S, Haque SA, Torres T, Nuesch F, Geiger T, Zakeeruddin SM, Gratzel M, Nazeeruddin MK (2009) PbS and US quantum dot-sensitized solid-state solar cells: old concepts, new results. *Adv Funct Mater* 19(17):2735–2742
60. Lee HJ, Chen P, Moon SJ, Sauvage F, Sivula K, Bessho T, Gamelin DR, Comte P, Zakeeruddin SM, Il Seok S, Gratzel M, Nazeeruddin MK (2009) Regenerative PbS and CdS quantum dot sensitized solar cells with a cobalt complex as hole mediator. *Langmuir* 25(13):7602–7608

61. Lu P, Shi ZW, Walker AV (2010) Selective formation of monodisperse CdSe nanoparticles on functionalized self-assembled monolayers using chemical bath deposition. *Electrochim Acta* 55(27):8126–8134
62. Gorer S, Hodes G (1994) Quantum-size effects in the study of chemical solution deposition mechanisms of semiconductor-films. *J Phys Chem* 98(20):5338–5346
63. Sudhagar P, Gonzalez-Pedro V, Mora-Sero I, Fabregat-Santiago F, Bisquert J, Kang YS (2012) Interfacial engineering of quantum dot-sensitized TiO₂ fibrous electrodes for futuristic photoanodes in photovoltaic applications. *J Mater Chem* 22(28):14228–14235
64. Niitsoo O, Sarkar SK, Pejoux C, Ruhle S, Cahen D, Hodes G (2006) Chemical bath deposited CdS/CdSe-sensitized porous TiO₂ solar cells. *J Photochem Photobiol A-Chem* 181(2–3):306–313
65. Heo JH, Im SH, Kim HJ, Boix PP, Lee SJ, Seok SI, Mora-Sero I, Bisquert J (2012) Sb₂S₃-sensitized photoelectrochemical cells: open circuit voltage enhancement through the introduction of poly-3-hexylthiophene interlayer. *J Phys Chem C* 116(39):20717–20721
66. Lim CS, Im SH, Rhee JH, Lee YH, Kim HJ, Maiti N, Kang Y, Chang JA, Nazeeruddin MK, Gratzel M, Seok SI (2012) Hole-conducting mediator for stable Sb₂S₃-sensitized photoelectrochemical solar cells. *J Mater Chem* 22(3):1107–1111
67. Chang JA, Im SH, Lee YH, Kim H-J, Lim C-S, Heo JH, Seok SI (2012) Panchromatic photon-harvesting by hole-conducting materials in inorganic-organic heterojunction sensitized-solar cell through the formation of nanostructured electron channels. *Nano Lett* 12(4):1863–1867
68. Chang JA, Rhee JH, Im SH, Lee YH, Kim H-J, Seok SI, Nazeeruddin MK, Grätzel M (2010) High-performance nanostructured inorganic—Organic heterojunction solar cells. *Nano Lett* 10(7):2609–2612
69. Rodenas P, Song T, Sudhagar P, Marzari G, Han H, Badia-Bou L, Gimenez S, Fabregat-Santiago F, Mora-Sero I, Bisquert J, Paik U, Kang YS (2013) Quantum dot based heterostructures for unassisted photoelectrochemical hydrogen generation. *Adv Energy Mater* 3(2):176–182
70. Sudhagar P, Song T, Lee DH, Mora-Sero I, Bisquert J, Laudenslager M, Sigmund WM, Park WI, Paik U, Kang YS (2011) High open circuit voltage quantum dot sensitized solar cells manufactured with ZnO Nanowire arrays and Si/ZnO branched hierarchical structures. *J Phys Chem Lett* 2(16):1984–1990
71. Samadpour M, Gimenez S, Boix PP, Shen Q, Calvo ME, Taghavinia N, Zad AI, Toyoda T, Miguez H, Mora-Sero I (2012) Effect of nanostructured electrode architecture and semiconductor deposition strategy on the photovoltaic performance of quantum dot sensitized solar cells. *Electrochim Acta* 75:139–147
72. Niesen TP, De Guire MR (2002) Review: deposition of ceramic thin films at low temperatures from aqueous solutions. *Solid State Ionics* 151(1–4):61–68
73. Pathan HM, Lokhande CD (2004) Deposition of metal chalcogenide thin films by successive ionic layer adsorption and reaction (SILAR) method. *Bull Mater Sci* 27(2):85–111
74. Froment M, Cachet H, Essaïdi H, Maurin G, Cortes R (1997) Metal chalcogenide semiconductors growth from aqueous solutions. *Pure Appl Chem* 69(1):77–82
75. Pawar SM, Pawar BS, Kim JH, Joo OS, Lokhande CD (2011) Recent status of chemical bath deposited metal chalcogenide and metal oxide thin films. *Curr Appl Phys* 11(2):117–161
76. Lee H, Wang MK, Chen P, Gamelin DR, Zakeeruddin SM, Gratzel M, Nazeeruddin MK (2009) Efficient CdSe quantum dot-sensitized solar cells prepared by an improved successive ionic layer adsorption and reaction process. *Nano Lett* 9(12):4221–4227
77. Hossain MA, Jennings JR, Shen C, Pan JH, Koh ZY, Mathews N, Wang Q (2012) CdSe-sensitized mesoscopic TiO₂ solar cells exhibiting > 5 % efficiency: redundancy of CdS buffer layer. *J Mater Chem* 22(32):16235–16242
78. O'Mahony FTF, Lutz T, Guijarro N, Gomez R, Haque SA (2012) Electron and hole transfer at metal oxide/Sb₂S₃/spiro-OMeTAD heterojunctions. *Energy Environ Sci* 5(12):9760–9764

79. Sahu SN (1989) Aqueous electrodeposition of Inp semiconductor-Films. *J Mater Sci Lett* 8(5):533–534
80. Allongue P, Souteyrand E (1989) Semiconductor electrodes modified by electrodeposition of discontinuous metal-films. I. Role of the film morphology. *J Electroanal Chem* 269(2):361–374
81. Switzer JA, Hung CJ, Bohannan EW, Shumsky MG, Golden TD, VanAken DC (1997) Electrodeposition of quantum-confined metal semiconductor nanocomposites. *Adv Mater* 9(4):334–000
82. Riveros G, Gomez H, Henriquez R, Schrebler R, Marotti RE, Dalchiele EA (2001) Electrodeposition and characterization of ZnSe semiconductor thin films. *Sol Energy Mater Sol Cells* 70(3):255–268
83. Rajeshwar, K.; deTacconi, N. R., Electrodeposition and characterization of nanocrystalline semiconductor films. *Semiconductor Nanoclusters- Physical, Chemical, and Catalytic Aspects* 1997, 103, 321-351
84. Lévy-Clément C, Katty A, Bastide S, Zenia F, Mora I, Munoz-Sanjose V (2002) A new CdTe/ZnO columnar composite film for Eta solar cells. *Physica E* 14:229–232
85. Lévy-Clément C, Tena-Zaera R, Ryan MA, Katty A, Hodes G (2005) CdSe sensitized p-CuSCN/Nanowire n-ZnO heterojunctions. *Adv Mater* 17:1512–1515
86. Lincot D (2005) Electrodeposition of semiconductors. *Thin Solid Films* 487(1–2):40–48
87. Savadogo O (1998) Chemically and electrochemically deposited thin films for solar energy materials. *Sol Energy Mater Sol Cells* 52(3–4):361–388
88. Behar D, Rubinstein I, Hodes G, Cohen S, Cohen H (1999) Electrodeposition of CdS quantum dots and their optoelectronic characterization by photoelectrochemical and scanning probe spectroscopies. *Superlattices Microstruct* 25(4):601–613
89. Han W, Cao LY, Huang JF, Wu JP (2009) Influence of pH value on PbS thin films prepared by electrodeposition. *Mater Technol* 24(4):217–220
90. Fernandes VC, Salvietti E, Loglio F, Lastraioli E, Innocenti M, Mascaro LH, Foresti ML (2009) Electrodeposition of PbS multilayers on Ag(111) by ECALE. *J Appl Electrochem* 39(11):2191–2197
91. Takahashi M, Ohshima Y, Nagata K, Furuta S (1993) Electrodeposition of Pbs films from acidic solution. *J Electroanal Chem* 359(1–2):281–286
92. Fantini MCA, Moro JR, Decker F (1988) Electrodeposition of Cdse films on Sno2-F coated glass. *Solar Energy Mater* 17(4):247–255
93. Kutzmutz S, Lang G, Heusler KE (2001) The electrodeposition of CdSe from alkaline electrolytes. *Electrochim Acta* 47(6):955–965
94. Anderson MA, Gorer S, Penner RM (1997) A hybrid electrochemical/chemical synthesis of supported, luminescent cadmium sulfide nanocrystals. *J Phys Chem B* 101(31):5895–5899
95. Song MY, Kim DK, Ihn KJ, Jo SM, Kim DY (2004) Electrospun TiO₂ electrodes for dye-sensitized solar cells. *Nanotechnology* 15(12):1861–1865
96. Fujihara K, Kumar A, Jose R, Ramakrishna S, Uchida S (2007) Spray deposition of electrospun TiO₂ nanorods for dye-sensitized solar cell. *Nanotechnology* 18(36)
97. Archana PS, Jose R, Vijila C, Ramakrishna S (2009) Improved electron diffusion coefficient in electrospun TiO₂ nanowires. *J Phys Chem C* 113(52):21538–21542
98. Ghadiri E, Taghavinia N, Zakeeruddin SM, Grätzel M, Moser JE (2010) Enhanced electron collection efficiency in dye-sensitized solar cells based on nanostructured TiO₂ hollow fibers. *Nano Lett* 10(5):1632–1638
99. Joshi P, Zhang LF, Davoux D, Zhu ZT, Galipeau D, Fong H, Qiao QQ (2010) Composite of TiO₂ nanofibers and nanoparticles for dye-sensitized solar cells with significantly improved efficiency. *Energy Environ Sci* 3(10):1507–1510
100. Martins A, Reis RL, Neves NM (2008) Electrospinning: processing technique for tissue engineering scaffolding. *Int Mater Rev* 53(5):257–274
101. Bhardwaj N, Kundu SC (2010) Electrospinning: a fascinating fiber fabrication technique. *Biotechnol Adv* 28(3):325–347

102. Ramaseshan R, Sundararajan S, Jose R, Ramakrishna S (2007) Nanostructured ceramics by electrospinning. *J Appl Phys* 102(11)
103. Yang SY, Nair AS, Jose R, Ramakrishna S (2010) Electrospun TiO₂ nanorods assembly sensitized by CdS quantum dots: a low-cost photovoltaic material. *Energy Environ Sci* 3(12):2010–2014
104. Song MY, Kim DK, Ihn KJ, Jo SM, Kim DY (2005) New application of electrospun TiO₂ solid-state dye-sensitized solar electrode to cells. *Synth Met* 153(1–3):77–80
105. Onozuka K, Ding B, Tsuge Y, Naka T, Yamazaki M, Sugi S, Ohno S, Yoshikawa M, Shiratori S (2006) Electrospinning processed nanofibrous TiO₂ membranes for photovoltaic applications. *Nanotechnology* 17(4):1026–1031
106. Sudhagar P, Jung JH, Park S, Sathyamoorthy R, Ahn H, Kang YS (2009) Self-assembled CdS quantum dots-sensitized TiO₂ nanospheroidal solar cells: Structural and charge transport analysis. *Electrochim Acta* 55(1):113–117
107. Samadpour M, Gimenez S, Zad AI, Taghavinia N, Mora-Sero I (2012) Easily manufactured TiO₂ hollow fibers for quantum dot sensitized solar cells. *Phys Chem Chem Phys* 14(2):522–528
108. Han H, Sudhagar P, Song T, Jeon Y, Mora-Sero I, Fabregat-Santiago F, Bisquert J, Kang YS, Paik U (2013) Three dimensional-TiO₂ nanotube array photoanode architectures assembled on a thin hollow nanofibrous backbone and their performance in quantum dot-sensitized solar cells. *Chem Commun* 49(27):2810–2812
109. Li ZD, Zhou Y, Bao CX, Xue GG, Zhang JY, Liu JG, Yu T, Zou ZG (2012) Vertically building Zn₂SnO₄ nanowire arrays on stainless steel mesh toward fabrication of large-area, flexible dye-sensitized solar cells. *Nanoscale* 4(11):3490–3494
110. Tao RH, Wu JM, Xue HX, Song XM, Pan X, Fang XQ, Fang XD, Dai SY (2010) A novel approach to titania nanowire arrays as photoanodes of back-illuminated dye-sensitized solar cells. *J Power Sources* 195(9):2989–2995
111. Law M, Greene LE, Johnson JC, Saykally R, Yang PD (2005) Nanowire dye-sensitized solar cells. *Nat Mater* 4(6):455–459
112. Xu CK, Wu JM, Desai UV, Gao D (2011) Multilayer assembly of nanowire arrays for dye-sensitized solar cells. *J Am Chem Soc* 133(21):8122–8125
113. Liu XL, Lin J, Chen XF (2013) Synthesis of long TiO₂ nanotube arrays with a small diameter for efficient dye-sensitized solar cells. *Rsc Adv* 3(15):4885–4889
114. Lin J, Liu XL, Guo M, Lu W, Zhang GG, Zhou LM, Chen XF, Huang HT (2012) A facile route to fabricate an anodic TiO₂ nanotube-nanoparticle hybrid structure for high efficiency dye-sensitized solar cells. *Nanoscale* 4(16):5148–5153
115. Kang TS, Smith AP, Taylor BE, Durstock MF (2009) Fabrication of highly-ordered TiO₂ nanotube arrays and their use in dye-sensitized solar cells. *Nano Lett* 9(2):601–606
116. Xie ZB, Adams S, Blackwood DJ, Wang J (2008) The effects of anodization parameters on titania nanotube arrays and dye sensitized solar cells. *Nanotechnology* 19(40)
117. Shankar K, Bandara J, Paulose M, Wietasch H, Varghese OK, Mor GK, LaTempa TJ, Thelakkat M, Grimes CA (2008) Highly efficient solar cells using TiO₂ nanotube arrays sensitized with a donor-antenna dye. *Nano Lett* 8(6):1654–1659
118. Zhang QF, Cao GZ (2011) Nanostructured photoelectrodes for dye-sensitized solar cells. *Nano Today* 6(1):91–109
119. Xu F, Dai M, Lu YN, Sun LT (2010) Hierarchical ZnO nanowire-nanosheet architectures for high power conversion efficiency in dye-sensitized solar cells. *J Phys Chem C* 114(6):2776–2782
120. Ko SH, Lee D, Kang HW, Nam KH, Yeo JY, Hong SJ, Grigoropoulos CP, Sung HJ (2011) Nanoforest of hydrothermally grown hierarchical ZnO nanowires for a high efficiency dye-sensitized solar cell. *Nano Lett* 11(2):666–671
121. Cheng CW, Fan HJ (2012) Branched nanowires: synthesis and energy applications. *Nano Today* 7(4):327–343

122. Qiu JJ, Li XM, Gao XD, Gan XY, Weng BB, Li L, Yuan ZJ, Shi ZS, Hwang YH (2012) Branched double-shelled TiO₂ nanotube networks on transparent conducting oxide substrates for dye sensitized solar cells. *J Mater Chem* 22(44):23411–23417
123. Chen HY, Kuang DB, Su CY (2012) Hierarchically micro/nanostructured photoanode materials for dye-sensitized solar cells. *J Mater Chem* 22(31):15475–15489
124. Dai H, Zhou Y, Liu Q, Li ZD, Bao CX, Yu T, Zhou ZG (2012) Controllable growth of dendritic ZnO nanowire arrays on a stainless steel mesh towards the fabrication of large area, flexible dye-sensitized solar cells. *Nanoscale* 4(17):5454–5460
125. Bierman MJ, Jin S (2009) Potential applications of hierarchical branching nanowires in solar energy conversion. *Energy Environ Sci* 2(10):1050–1059
126. McCune M, Zhang W, Deng YL (2012) High efficiency dye-sensitized solar cells based on three-Dimensional multilayered ZnO nanowire arrays with “Caterpillarlike” structure. *Nano Lett* 12(7):3656–3662
127. Wu WQ, Lei BX, Rao HS, Xu YF, Wang YF, Su CY, Kuang DB (2013) Hydrothermal fabrication of hierarchically anatase TiO₂ nanowire arrays on FTO glass for dye-sensitized solar cells. *Sci Rep* 3
128. Sauvage F, Di Fonzo F, Bassi AL, Casari CS, Russo V, Divitini G, Ducati C, Bottani CE, Comte P, Graetzel M (2010) Hierarchical TiO₂ photoanode for dye-sensitized solar cells. *Nano Lett* 10(7):2562–2567
129. Tétreault N, Heiniger L-P, Stefik M, Labouchère PL, Arsenaault É, Nazeeruddin NK, Ozin GA, Grätzel M (2011) (Invited) Atomic layer deposition for novel dye-sensitized solar cells. *ECS Trans* 41(2):303–314
130. Xu CK, Wu JM, Desai UV, Gao D (2012) High-efficiency solid-state dye-sensitized solar cells based on TiO₂-coated ZnO nanowire arrays. *Nano Lett* 12(5):2420–2424
131. Halaoui LI, Abrams NM, Mallouk TE (2005) Increasing the conversion efficiency of dye-sensitized TiO₂ photoelectrochemical cells by coupling to photonic crystals. *J Phys Chem B* 109(13):6334–6342
132. Guldin S, Hüttner S, Kolle M, Welland ME, Müller-Buschbaum P, Friend RH, Steiner U, Tétreault N (2010) Dye-sensitized solar cell based on a three-dimensional photonic crystal. *Nano Lett* 10(7):2303–2309
133. Liu LJ, Karuturi SK, Su LT, Tok AIY (2011) TiO₂ inverse-opal electrode fabricated by atomic layer deposition for dye-sensitized solar cell applications. *Energy Environ Sci* 4(1):209–215
134. Choi JH, Kwon SH, Jeong YK, Kim I, Kim KH (2011) Atomic layer deposition of Ta-doped TiO₂ electrodes for dye-sensitized solar cells. *J Electrochem Soc* 158(6):B749–B753
135. King JS, Graugnard E, Summers CJ (2005) TiO₂ inverse opals fabricated using low-temperature atomic layer deposition. *Adv Mater* 17(8):1010–+
136. Chen JIL, von Freymann G, Choi SY, Kitaev V, Ozin GA (2008) Slow photons in the fast lane in chemistry. *J Mater Chem* 18(4):369–373
137. Yip C-H, Chiang Y-M, Wong C-C (2008) Dielectric band edge enhancement of energy conversion efficiency in photonic crystal dye-sensitized solar cell. *J Phys Chem C* 112(23):8735–8740
138. Shin JH, Kang JH, Jin WM, Park JH, Cho YS, Moon JH (2011) Facile synthesis of TiO₂ inverse opal electrodes for dye-sensitized solar cells. *Langmuir* 27(2):856–860
139. Han SH, Lee S, Shin H, Jung HS (2011) A quasi-inverse opal layer based on highly crystalline TiO₂ nanoparticles: a new light-scattering layer in dye-sensitized solar cells. *Adv Energy Mater* 1(4):546–550
140. Mihi A, Calvo ME, Anta JA, Miguez H (2008) Spectral response of opal-based dye-sensitized solar cells. *J Phys Chem C* 112(1):13–17
141. Nishimura S, Abrams N, Lewis BA, Halaoui LI, Mallouk TE, Benkstein KD, van de Lagemaat J, Frank AJ (2003) Standing wave enhancement of red absorbance and photocurrent in dye-sensitized titanium dioxide photoelectrodes coupled to photonic crystals. *J Am Chem Soc* 125(20):6306–6310

142. Yuan S, Huang H, Wang Z, Zhao Y, Shi L, Cai C, Li D (2013) Improved electron-collection performance of dye sensitized solar cell based on three-dimensional conductive grid. *J Photochem Photobiol A* 259:10–16
143. Cho CY, Moon JH (2012) Hierarchical twin-scale inverse opal TiO₂ electrodes for dye-sensitized solar cells. *Langmuir* 28(25):9372–9377
144. Kwak ES, Lee W, Park NG, Kim J, Lee H (2009) Compact inverse-opal electrode using non-aggregated TiO₂ nanoparticles for dye-sensitized solar cells. *Adv Funct Mater* 19(7):1093–1099
145. Toyoda T, Shen Q (2012) Quantum-dot-sensitized solar cells: effect of nanostructured TiO₂ morphologies on photovoltaic properties. *J Phys Chem Lett* 3(14):1885–1893
146. Diguna LJ, Shen Q, Kobayashi J, Toyoda T (2007) High efficiency of CdSe quantum-dot-sensitized TiO₂ inverse opal solar cells. *Appl Phys Lett* 91(2)
147. Shalom M, Dor S, Rühle S, Grinis L, Zaban A (2009) Core/CdS quantum dot/shell mesoporous solar cells with improved stability and efficiency using an amorphous TiO₂ coating. *J Phys Chem C* 113:3895–3898
148. Chakrapani V, Baker D, Kamat PV (2011) Understanding the role of the sulfide redox couple (S^{2-}/S_n^{2-}) in quantum dot-sensitized solar cells. *J Am Chem Soc* 133:9607–9615
149. Gonzalez-Pedro V, Sima C, Marzari G, Boix PP, Gimenez S, Shen Q, Ditttrich T, Mora-Sero I (2013) High performance PbS quantum dot sensitized solar cells exceeding 4 % efficiency: the role of metal precursors in the electron injection and charge separation. *Phys Chem Chem Phys*
150. Jovanovski V, González-Pedro V, Giménez S, Azaceta E, Cabañero G, Grande H, Tena-Zaera R, Mora-Seró I, Bisquert J (2011) A sulfide/polysulfide-based ionic liquid electrolyte for quantum dot-sensitized solar cells. *J Am Chem Soc* 133:20156–20159
151. Choné C, Larramona G (2007) French Patent 2899385, 05
152. Messina S, Nair MTS, Nair PK (2007) Antimony sulfide thin films in chemically deposited thin film photovoltaic cells. *Thin Solid Films* 515:5777–5782
153. Moon S-J, Itzhaik Y, Yum J-H, Zakeeruddin SM, Hodes G, Grätzel M (2010) Sb₂S₃ based mesoscopic solar cell using an organic hole conductor. *J Phys Chem Lett* 1:1524–1527
154. Im SH, Lim C-S, Chang JA, Lee YH, Maiti N, Kim H-J, Nazeeruddin MK, Grätzel M, Seok SI (2011) Toward interaction of sensitizer and functional moieties in hole-transporting materials for efficient semiconductor-sensitized solar cells. *Nano Lett* 11:4789–4793
155. Hodes G, Manassen J, Cahen D (1980) Electrocatalytic electrodes for the polysulfide redox system. *J Electrochem Soc* 127:544–549
156. Yang YY, Zhu LF, Sun HC, Huang XM, Luo YH, Li DM, Meng QB (2012) Composite counter electrode based on nanoparticulate PbS and carbon black: towards quantum dot-sensitized solar cells with both high efficiency and stability. *ACS Appl Mater Interfaces* 4(11):6162–6168
157. Sudhagar P, Ramasamy E, Cho W-H, Lee J, Kang YS (2011) Robust mesocellular carbon foam counter electrode for quantum-dot sensitized solar cells. *Electrochem Commun* 13(1):34–37
158. Yang, Z.; Chen, C.-Y.; Liu, C.-W.; Li, C.-L.; Chang, H.-T., Quantum Dot-Sensitized Solar Cells Featuring CuS/CoS Electrodes Provide 4.1 % Efficiency. *Advanced Energy Materials* 2011, 1, 259-264
159. Deng M, Huang S, Zhang Q, Li D, Luo Y, Shen Q, Toyoda T, Meng Q (2010) Screen-printed Cu₂S-based counter electrode for quantum-dot-sensitized solar cell. *Chem Lett* 39:1168–1170
160. Radich JG, Dwyer R, Kamat PV (2011) Cu₂S reduced graphene oxide composite for high-efficiency quantum dot solar cells. overcoming the redox limitations of S₂/Sn₂ at the counter electrode. *J Phys Chem Lett* 2:2453–2460
161. Santra PK, Kamat PV (2012) Mn-doped quantum dot sensitized solar cells: a strategy to boost efficiency over 5 %. *J Am Chem Soc* 134(5):2508–2511
162. Santra PK, Kamat PV (2012) Mn-doped quantum dot sensitized solar cells: a strategy to boost efficiency over 5 %. *J Am Chem Soc* 134(5):2508–2511

163. Samadpour M, Boix PP, Giménez S, Irají Zad A, Taghavinia N, Mora-Seró I, Bisquert J (2011) Fluorine treatment of TiO_2 for enhancing quantum dot sensitized solar cell performance. *J Phys Chem C* 115:14400–14407
164. Barea EM, Shalom M, Giménez S, Hod I, Mora-Seró I, Zaban A, Bisquert J (2010) Design of injection and recombination in quantum dot sensitized solar cells. *J Am Chem Soc* 132:6834–6839
165. de la Fuente MS, Sánchez RS, González-Pedro V, Boix PP, Mhaisalkar SG, Rincón ME, Bisquert J, Mora-Seró I (2013) Effect of organic and inorganic passivation in quantum-dot-sensitized solar cells. *J Phys Chem Lett* 4(9):1519–1525
166. Mora-Sero I, Bisquert J (2010) Breakthroughs in the development of semiconductor-sensitized solar cells. *J Phys Chem Lett* 1(20):3046–3052
167. Kamat PV, Tvrdý K, Baker DR, Radich JG (2010) Beyond photovoltaics: semiconductor nanoarchitectures for liquid-junction solar cells. *Chem Rev* 110(11):6664–6688
168. Burschka J, Pellet N, Moon S-J, Humphry-Baker R, Gao P, Nazeeruddin MK, Grätzel M (2013) Sequential deposition as a route to high-performance perovskite-sensitized solar cells. *Nature* (advance online publication)
169. Kagan CR, Mitzi DB, Dimitrakopoulos CD (1999) Organic-inorganic hybrid materials as semiconducting channels in thin-film field-effect transistors. *Science* 286:945–947
170. Kim H-S, Lee C-R, Im J-H, Lee K-B, Moehl T, Marchioro A, Moon S-J, Humphry-Baker R, Yum J-H, Moser JE, Grätzel M, Park N-G (2012) Lead iodide perovskite sensitized all-solid-state submicron thin film mesoscopic solar cell with efficiency exceeding 9 %. *Nat Sci Rep* 2(591):591
171. Baikie T, Fang Y, Kadro JM, Schreyer M, Wei F, Mhaisalkar SG, Graetzel M, Whitec TJ (2013) Synthesis and crystal chemistry of the hybrid perovskite $(\text{CH}_3\text{NH}_3)\text{PbI}_3$ for solid-state sensitized solar cell applications. *J Mater Chem A* 1:5628–5641
172. Im J-H, Lee C-R, Lee J-W, Park S-W, Park N-G (2011) 6.5 % efficient perovskite quantum-dot-sensitized solar cell†. *Nanoscale* 3:4088–4093
173. Kojima A, Teshima K, Shirai Y, Miyasaka T (2009) Organometal halide perovskites as visible-light sensitizers for photovoltaic cells. *J Am Chem Soc* 131(2):6050–6051
174. Lee MM, Teuscher J, Miyasaka T, Murakami TN, Snaith HJ (2012) Efficient hybrid solar cells based on meso-superstructured organometal halide perovskites. *Science* 338:643–647
175. Etgar L, Gao P, Xue Z, Peng Q, Chandiran AK, Liu B, Nazeeruddin MK, Grätzel M (2012) Mesoscopic $\text{CH}_3\text{NH}_3\text{PbI}_3/\text{TiO}_2$ heterojunction solar cells. *J Am Chem Soc* 134:17396–17399
176. Heo JH, Im SH, Noh JH, Mandal TN, Lim C-S, Chang JA, Lee YH, Kim H-J, Sarkar A, Nazeeruddin MK, Grätzel M, Seok SI (2013) Efficient inorganic-organic hybrid heterojunction solar cells containing perovskite compound and polymeric hole conductors. *Nat Photonics* 7:486–491
177. Kim H-S, Lee J-W, Yantara N, Boix PP, Kulkarni SA, Mhaisalkar S, Grätzel M, Park N-G (2013) High efficiency solid-state sensitized solar cell-based on submicrometer rutile TiO_2 nanorod and $\text{CH}_3\text{NH}_3\text{PbI}_3$ perovskite sensitizer. *Nano Lett* 16:2412–2417
178. Noh JH, Im SH, Heo JH, Mandal TN, Seok SI (2013) Chemical management for colorful, efficient, and stable inorganic-organic hybrid nanostructured solar cells. *Nano Lett* 7:1764–1769
179. Qiu J, Qiu Y, Yan K, Zhong M, Mu C, Yan H, Yang S (2013) All-solid-state hybrid solar cells based on a new organometal halide perovskite sensitizer and one-dimensional TiO_2 nanowire arrays. *Nanoscale* 5:3245–3248
180. Ball JM, Lee MM, Hey A, Snaith H (2013) Low-temperature processed mesosuperstructured to thin-film perovskite solar cells. *Energy Environ Sci* 6:1739–1743
181. Edri E, Kirmayer S, Cahen D, Hodes G (2013) High open-circuit voltage solar cells based on organic-inorganic lead bromide perovskite. *J Phys Chem* 4:897–902
182. Kim H-S, Mora-Sero I, Gonzalez-Pedro V, Fabregat-Santiago F, Juarez-Perez EJ, Park N-G, Bisquert J (2013) Mechanism of carrier accumulation in perovskite thin absorber solar cells. *Nat Commun* 4:2242

183. Sauvage F, Davoisne C, Philippe L, Elias J (2012) Structural and optical characterization of electrodeposited CdSe in mesoporous anatase TiO₂ for regenerative quantum-dot-sensitized solar cells. *Nanotechnology* 23(39)
184. Bang JH, Kamat PV (2010) Solar cells by design: photoelectrochemistry of TiO₂ nanorod arrays decorated with CdSe. *Adv Funct Mater* 20(12):1970–1976
185. Boix PP, Lee YH, Fabregat-Santiago F, Im SH, Mora-Seró I, Bisquert J, Seok SI (2012) From flat to nanostructured photovoltaics: balance between thickness of the absorber and charge screening in sensitized solar cells. *ACS Nano* 6(1):873–880
186. An H, Ahn HJ (2013) Fabrication of wrinkled Nb-doped TiO₂ nanofibres via electrospinning. *Mater Lett* 93:88–91
187. Herman I, Yeo J, Hong S, Lee D, Nam KH, Choi JH, Hong WH, Lee D, Grigoropoulos CP, Ko SH (2012) Hierarchical weeping willow nano-tree growth and effect of branching on dye-sensitized solar cell efficiency. *Nanotechnology* 23(19)
188. Fabregat-Santiago F, Garcia-Belmonte G, Mora-Seró I, Bisquert J (2011) Characterization of nanostructured hybrid and organic solar cells by impedance spectroscopy. *Phys Chem Chem Phys* 13:9083–9118
189. Boix PP, Larramona G, Jacob A, Delatouche B, Mora-Seró I, Bisquert J (2012) Hole transport and recombination in all-solid Sb₂S₃-sensitized TiO₂ solar cells using CuSCN as hole transporter. *J Phys Chem C* 116(1):1579–1587